

Sedimentary response to a collision orogeny recorded in detrital zircon provenance of Greater Caucasus foreland basin sediments

Alexander R. Tye¹  | Nathan A. Niemi¹  | Rafiq T. Safarov² |
Fakhraddin A. Kadirov² | Gulam R. Babayev²

¹Department of Earth and Environmental Sciences, University of Michigan, Ann Arbor, MI, USA

²Institute of Geology and Geophysics, Azerbaijan National Academy of Sciences, Baku, Azerbaijan

Correspondence

Alexander R. Tye, Department of Earth and Environmental Sciences, University of Michigan, Ann Arbor, MI 48109, USA.
Email: alextye@umich.edu

Abstract

The Greater Caucasus orogen on the southern margin of Eurasia is hypothesized to be a young collisional system and may present an opportunity to probe the structural, sedimentary and geodynamic effects of continental collision. We present detrital zircon U-Pb age data from the Caucasus region that constrain changes in sediment routing and source exposure during the late Cenozoic convergence and collision between the Greater Caucasus orogen and the Lesser Caucasus, an arc terrane on the lower plate of the system. During Oligocene to Middle Miocene time, following the initiation of deformation within the Greater Caucasus, marine sandstones and shales were deposited between the Greater and Lesser Caucasus, and detrital zircon age data suggest no mixing of Greater Caucasus and Lesser Caucasus detritus. During Middle to Late Miocene time, Greater Caucasus detritus was deposited onto the Lesser Caucasus basin margin, and terrestrial, largely conglomeratic, sedimentation began between the Greater and Lesser Caucasus. Around 5.3 Ma, upper plate exhumation rates increased and shortening migrated to pro- and retro-wedge fold-thrust belts, coinciding with the initiation of foreland basin erosion. Sediment composition, provenance and structural data from the orogen together suggest the existence of a wide (230–280 km) marine basin that was progressively closed during Oligocene to Late Miocene time, probably by subduction/lithospheric underthrusting beneath the Greater Caucasus, followed by initiation of collision between the Lesser Caucasus arc terrane and the Greater Caucasus in Late Miocene to Pliocene time. The pace of the transition from hypothesized subduction to collision in the Caucasus is consistent with predictions from numerical modeling for a system with moderate convergence rates (<13 mm/yr) and hot lower plate continental lithosphere. Basement crystallization histories implied by our detrital zircon age data suggest the presence of two pre-Jurassic sutures between stable Eurasia and the Lesser Caucasus, which likely guided later deformation.

KEYWORDS

Caucasus, collision, detrital zircon, provenance, Tethys

1 | Introduction

The collision of two continents following the closure of an intervening ocean basin is a key element in the plate tectonic cycle (e.g. Nance, Murphy, & Santosh, 2014). The transition from subduction to collision, where lower plate buoyancy or other factors inhibit the downward motion of subducting lithosphere into the mantle, constitutes a major change in the balance of forces acting on an orogen (Beaumont, Ellis, Hamilton, & Fullsack, 1996; Duretz, Gerya, & May, 2011; Duretz, Schmalholz, & Gerya, 2012; Regard, Faccenna, Martinod, Bellier, & Thomas, 2003). The initiation of collision has been hypothesized to affect topography (e.g. England & Houseman, 1986), plate kinematics (Dewey, Helman, Knott, Turco, & Hutton, 1989; Patriat & Achache, 1984) and climate (e.g. Edmond, 1992; Jagoutz, Macdonald, & Royden, 2016; Molnar, Boos, & Battisti, 2010). Observations from numerous orogens and modelling studies show that the transition from subduction to collision is a complex and diachronous process, beginning with the entrance of continental or transitional lithosphere into a subduction zone (Chung et al., 2005; Klootwijk, Conaghan, & Powell, 1985; Lee & Lawver, 1995; Madanipour, Ehlers, Yassaghi, & Enkelmann, 2017; Regard et al., 2003), and subsequently involving diverse effects such as accretion of large parts of the lower plate, locking of the trench and development of fold and thrust belts, slowing of convergence and/or initiation of far-field deformation (Cowgill et al., 2016; Lee & Lawver, 1995; Regard et al., 2003; Toussaint, Burov, & Avouac, 2004; van Hinsbergen et al., 2012). In order to understand orogenic mass balance and the effects of collision on topography, climate, and plate kinematics, we need well-preserved records of the transition from subduction to collision (e.g. DeCelles, Kapp, Gehrels, & Ding, 2014; Zhuang et al., 2015, and references therein).

Foreland basin stratigraphic records of collisional orogens are commonly used to constrain the timing of collision (Dewey & Mange, 1999; Ding, Kapp & Wan, 2005; Weislogel et al., 2006; Zagorevski & van Staal, 2011) via dating of events such as initial arrival of upper plate detritus on a lower plate continental margin (Garzanti, Baud, & Mascle, 1987; Hu, Garzanti, Moore, & Raffi, 2015; Najman et al., 2010; Koshnaw, Stockli, & Schlunegger, 2019), cessation of marine sedimentation (Garzanti et al., 1987; Najman et al., 2010) and initiation of foreland basin subsidence (Ershov et al., 2003; Fakhari, Axen, Horton, Hassanzadeh, & Amini, 2008). However, interpretation of foreland basins in collisional tectonic systems is complicated by multiple factors including evolving source areas (Axen, Lam, Grove, Stockli, & Hassanzadeh, 2001), changing topography (Pusok & Kaus, 2015) and varying base levels (Krijgsman, Hilgen, Raffi, Sierro, & Wilson, 1999). Preservation of stratigraphic and other (e.g. thermochronometric, structural and kinematic) records is also an issue in mature collisional orogens (e.g.

Highlights

- Detrital zircon U-Pb ages record changes to sediment routing and source exposure during Caucasus collision.
- Upper plate detritus first deposited on lower plate basin margin between 15 and 5.3 Ma
- 5.3 Ma transition to foreland non-deposition and longitudinal transport of mixed upper- and lower-plate detritus
- Foreland non-deposition coincident with rise in upper-plate exhumation, foreland fold-thrust belt deformation

Hu et al., 2015). In the case of one mature collision zone, the India–Asia collision, diachronous transitions in foreland basin sedimentation in several studied stratigraphic sections have historically led to interpretations of collisional ages that differed from one another by up to 10 Myr (e.g. DeCelles et al., 2004; DeCelles et al., 2014; Hu, Sinclair, Wang, Jiang, & Wu, 2012; Hu et al., 2015; Najman et al., 2010; Wu et al., 2014; Zhuang et al., 2015). Thus, there is an ongoing need to better understand the stratigraphic record of initial collision and its spatial and temporal variation within a foreland basin system.

The optimal setting for investigating the sedimentary response to the initiation of collision is an orogen where collision began recently, so that independent constraints on the structural and kinematic evolution of the orogen are available. There are several examples of orogens thought to be undergoing the initial stages of collision where the sedimentary response to collision could be probed, including Taiwan (e.g. Teng, 1990), Timor (Carter, Audley-Charles, & Barber, 1976; Duffy, Quigley, Harris, & Ring, 2013; Tate et al., 2015) and the Caucasus (Mumladze et al., 2015; Philip, Cisternas, Gvishiani, & Gorshkov, 1989). Of these, the Caucasus is unique in that the basin in between the two colliding continents is currently non-marine, permitting ease of access to the foreland basin strata of interest. In addition, published marine magnetic anomaly, geodetic, structural and thermochronometric analyses constrain the kinematics of the Caucasus and the surrounding region during the transition from subduction to collision (Austermann & Iaffaldano, 2013; Avdeev & Niemi, 2011; Cowgill et al., 2016; Kadirov et al., 2012; Kadirov et al., 2015; Reilinger et al., 2006; van der Boon et al., 2018; van Hinsbergen et al., 2020; Vincent et al., 2020). The goal of this study is to derive from the stratigraphic records available in the Caucasus a preliminary, coupled sedimentary and kinematic framework of collision for further development and comparison with other orogens.

In this paper, we first develop a hypothesis of the sedimentary response to the early stages of collision. We then present a new detrital zircon U-Pb age dataset from the Caucasus to probe erosion, sediment routing and deposition in a natural example of this phase of the plate tectonic cycle. We characterize zircon U-Pb age signatures of potential sources of Cenozoic sediment by using targeted modern river samples. By comparing source age signatures to detrital zircon ages in samples from three foreland basin sections distributed along strike, we investigate the dispersal of sediment from upland sources into the basin between the Greater and Lesser Caucasus from the Oligocene to Quaternary. We combine this zircon U-Pb age dataset with published stratigraphy for the three sampled sections and published thermochronometric (Avdeev & Niemi, 2011; Vincent et al., 2020), geodetic (Kadirov et al., 2012, 2015; Reilinger et al., 2006; Sokhadze et al., 2018) and structural (Banks, Robinson, & Williams, 1997; Cowgill et al., 2016; Forte, Cowgill, Murtuzayev, Kangarli, & Stoica, 2013; Sobornov, 1994) records to correlate sedimentary changes with the structural evolution of the orogen and explore implications for collision. We also discuss zircon age distributions of regional basement domains and implications for the distribution of sutures along the southern margin of Eurasia, which may have guided later localization of deformation.

2 | HYPOTHESIZED RESPONSE OF FORELAND BASIN SEDIMENTATION TO EARLY COLLISION

Modelling and field observations provide perspectives on possible effects of the initiation of collision on an orogen (Beaumont et al., 1996; Garzanti et al., 1987; Gürer & van

Hinsbergen, 2019; Lallemand, Malavieille, & Calassou, 1992; Regard et al., 2003; Tricart, 1984; Toussaint et al., 2004), from which we hypothesize the effects on sedimentation between the colliding continental blocks (Figure 1). During pre-collisional subduction, an accretionary prism may grow on the basin margin above a subduction zone, marine sedimentation occurs in the basin and upper plate sediment may be deposited onto the lower plate as it enters the subduction zone (Figure 1a; Karig & Sharman, 1975). If convergence continues, the lower plate continental margin will eventually enter the subduction zone and fragments of the lower plate are likely to be accreted to the upper plate (Figure 1b; DeCelles et al., 2014; Tricart, 1984). Further continental subduction increases lower plate thickness and buoyancy, potentially driving further accretion and accelerating upper plate rock uplift (Beaumont et al., 1996; Lallemand et al., 1992; Toussaint et al., 2004) and narrowing and uplifting the basin between the two continents (Figure 1c). The increasing buoyancy of the incoming lower plate may drive locking of the subduction zone megathrust and migration of shortening to pro- and retrowedge fold and thrust belts (Beaumont et al., 1996; Toussaint et al., 2004). Increasing lower plate thickness and forward propagation of thrust belts will decrease accommodation between the two continental blocks and ultimately lead to erosive conditions in the basin along the plate boundary (e.g. DeCelles & Giles, 1996; Soria, Fernandez, & Viseras, 1999).

Along-strike variations in buoyancy, structural style and topography of an incipient collision zone are greatly influenced by the geometry of the lower plate continent (e.g. Gürer & van Hinsbergen, 2019). At the initial point of contact between the two colliding continents, the foreland basin is expected to undergo uplift and deformation. However, along-strike plate geometries may temporarily preserve lower elevation marine or non-marine basins where the converging continents are not yet

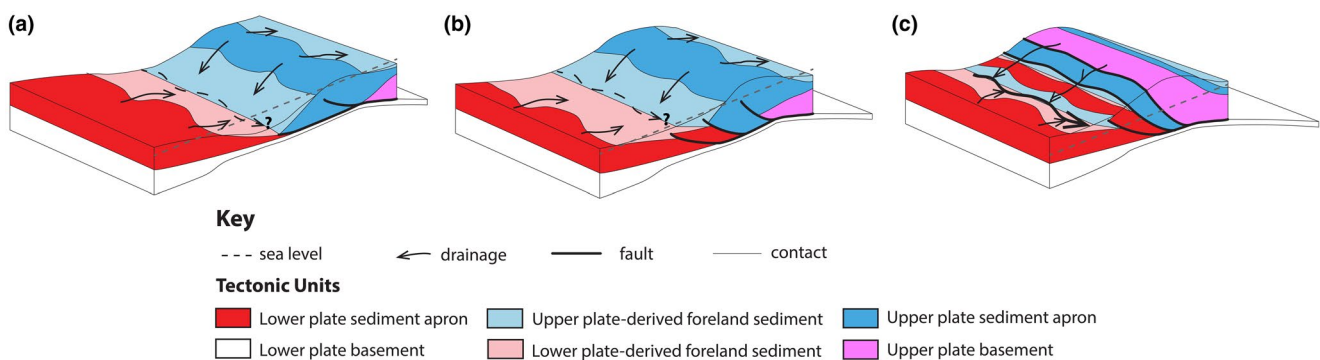


FIGURE 1 Effects of the transition from subduction to collision on an orogen and its foreland basin (see Section 2 for complete discussion). (a) Narrowing of an ocean basin is accommodated by subduction, resulting in the formation of an accretionary prism above the subduction zone. (b) Lower plate continental slope enters the subduction zone, resulting in accretion of lower plate stratigraphy along a new frontal thrust. (c) Further convergence drives locking of the subduction zone, increased slip on the frontal thrust, and foreland basin deformation and uplift. Foreland basin uplift causes erosion and sediment transport via a longitudinal drainage network. (c) the current state of the western Caucasus, whereas the eastern Caucasus is in an intermediate state between (b) and (c).

in contact (e.g. Şengör, 1976). Tectonic uplift and closure of the foreland basin at the locus of collision is likely to increase the sediment supply of longitudinal drainages that convey sediment from the locus of collision to lower elevation sections of the basin along strike (Figure 1c; Malkowski, Schwartz, Sharman, Sickmann, & Graham, 2017). As collision continues, further shortening will result in the exposure of the lower portion of the prism, and accelerated upper plate rock uplift rates will lead to the exposure of deeper crustal levels (Figure 1c; Beaumont et al., 1996; Toussaint et al., 2004).

The predicted responses of the foreland basin to early collision include shallowing and a transition from marine to terrestrial to erosive conditions (Figure 1b-c); erosion and deposition of material from deeper crustal levels of the orogen (Figure 1c); and longitudinal drainage away from the locus of initial collision (Figure 1c). The Caucasus provides a natural setting in which to test whether these expected effects are observed and to constrain the relationships between these effects and the structural and kinematic changes that accompany collision.

3 | GEOLOGICAL BACKGROUND

The Caucasus region is located on the southern margin of Eurasia, within the Arabia–Eurasia collision zone (Figure 2a). To the immediate north of the Caucasus lies the Scythian platform (Natal'in & Şengör, 2005; Saintot, Stephenson, et al., 2006), which is bordered to its north by stable Eurasia (Figure 2a; Allen, Morton, Fanning, Ismail-Zadeh, & Kroonenberg, 2006; Bogdanova et al., 2008). To the south of the Caucasus lies the Turkish–Iranian plateau, which is demarcated from stable Arabia to its south by the Bitlis–Zagros suture, the Arabia–Eurasia plate boundary (Figure 2a; Copley & Jackson, 2006; Şengör & Kidd, 1979; Şengör & Yılmaz, 1981).

The Caucasus region consists of two parallel, WNW-striking mountain ranges, the Greater Caucasus (~1200 km long) and the Lesser Caucasus (~500 km long; Figure 2b), separated by a longitudinal drainage network. West of 43° E, the Greater Caucasus is separated from the Lesser Caucasus by the Rioni basin, in which the Rioni River flows west to the Black Sea (Figure 2a). Between 43° E and 45° E, a contiguous band of elevated topography runs between the Greater and Lesser Caucasus (Figure 2d). East of 45° E, the Greater Caucasus is separated from the Lesser Caucasus by the Kura basin, in which the Kura River flows east to the Caspian Sea (Figure 2a). The current drainage network of the Greater Caucasus is consistent with the final step of our conceptual model of collision (Figure 1c).

3.1 | Tectonic setting and history

The present tectonic setting of the Caucasus is constrained by seismic and geodetic data (Figure 2b,c). Deep earthquakes

>50 km beneath the eastern Greater Caucasus suggest the presence of a north-dipping subducting slab beneath the range (Mellors et al., 2012; Mumladze et al., 2015), and GPS convergence rates of 10–12 mm/yr accommodated along the northern margin of the Kura basin are consistent with inferences that subduction is currently active (Kadirov et al., 2012, 2015; Reilinger et al., 2006). Seismic tomography indicates the presence of a high-velocity body in the upper mantle beneath the eastern Greater Caucasus interpreted as subducted or underthrust lithosphere (Skobeltsyn et al., 2014). The Lesser Caucasus mountains are on the lower plate of this subduction system, and the Kura basin separates the eastern Greater Caucasus from the Lesser Caucasus and its eastern extension, the Talysh (Figure 2b,c). In the western Greater Caucasus, range-normal GPS convergence rates of 3–4 mm/yr (Kadirov et al., 2015; Reilinger et al., 2006; Sokhadze et al., 2018), rapid exhumation (Avdeev & Niemi, 2011; Vincent et al., 2020) and contiguous elevated topography between the Greater and Lesser Caucasus (Figure 2d) suggest that this part of the range is currently undergoing collision with the Lesser Caucasus (Figure 2b,c). The combination of ongoing collision inferred in the western Caucasus and active subduction in the eastern Caucasus suggests that the orogen may be transitioning diachronously from subduction to collision, with the western part of the range at a more advanced stage of this transition than the eastern part of the range (Figure 2b; Mumladze et al., 2015). Active fold and thrust belts are located on both the pro- (Banks et al., 1997; Forte, Cowgill, Bernardin, Kreylos, & Hamann, 2010; Forte et al., 2013) and retro-wedge (Sobornov, 1994, 1996) sides of the orogen.

The Caucasus region has a complex deformation history. The southern Eurasian margin was affected by successive episodes of subduction, terrane accretion, and rifting throughout the Phanerozoic that are thought to have generated significant lithospheric heterogeneity in the region (e.g. Şengör, 1984; Stampfli, 2013). The regional pre-Jurassic tectonic history remains uncertain, in part due to the lack of exposure of rocks old enough to record this history (e.g. Natal'in & Şengör, 2005; Saintot, Stephenson, et al., 2006). Most of the exposed bedrock in the Greater and Lesser Caucasus was deposited in an intra-arc or backarc basin environment during Jurassic to Eocene time (Figure 2b; Alizadeh, Guliyev, Kadirov, & Eppelbaum, 2016; Nalivkin, 1976). During this period, the Lesser Caucasus constituted an active volcanic arc that extended west into the Pontides and east into Iran above the north-dipping subducting slab of Neotethys (e.g. Adamia, Zakariadze, et al., 2011; Rolland, Sosson, Adamia, & Sadrade, 2011; Sosson et al., 2010). Concomitant with subduction and arc volcanism, a system of backarc and forearc basins opened parallel to the arc, including the Black Sea basins, the South Caspian basin, and the Greater Caucasus basin,

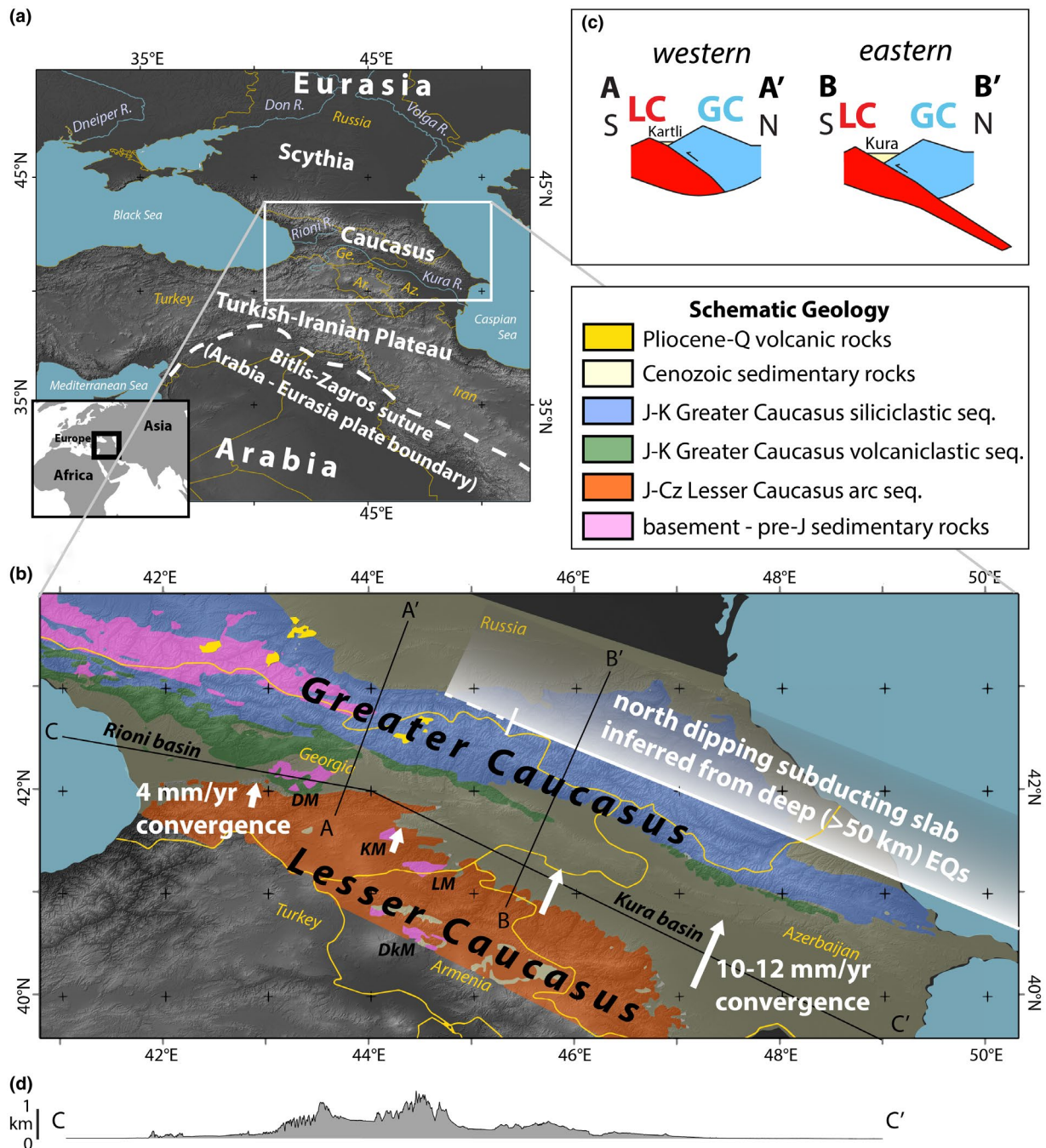


FIGURE 2 Location and tectonic setting of the Caucasus. (a) The Caucasus region is located on the southern margin of Eurasia in the Arabia-Eurasia collision zone. (b) The Caucasus region consists of the WNW-striking Greater Caucasus and Lesser Caucasus, which are converging towards one another. Schematic GPS convergence rates (Kadirov et al., 2015; Reilinger et al., 2006) between the Greater and Lesser Caucasus and extent of a north-dipping subducting slab inferred from deep earthquakes (Mellors et al., 2012; Mumladze et al., 2015) are shown in white. Key tectonic units are shown in colour with key to the upper right (see further discussion in Section 3.2). Abbreviated names of geologic features: DM—Dzirula Massif, KM—Khrami Massif, LM—Loki Massif, DkM—Dzarkuniatz Massif. Black lines show locations of cross sections (A-A', B-B') in (c) and topographic profile (C-C') in (d). (c) Schematic cross sections across the western (A-A') and eastern (B-B') Greater Caucasus. (d) Foreland basin topographic profile along strike of the Greater Caucasus (C-C').

which opened to the north of the Lesser Caucasus and is where most of the sedimentary bedrock presently exposed in the Greater Caucasus was originally deposited (e.g. Adamia, Zakariadze, et al., 2011; van Hinsbergen et al., 2020; Vincent, Braham, Lavrishchev, Maynard, & Harland,

2016; Zonenshain & Le Pichon, 1986). Extant basins that opened during this period are inferred to be floored by oceanic crust (Knapp, Knapp, & Connor, 2004; Nikishin et al., 2015) or transitional crust with a composition similar to mafic lower continental crust (Mangino & Priestley, 1998).

The composition of the basement of the Greater Caucasus basin is poorly constrained and is the subject of controversy, with both an oceanic composition and a thinned, mafic continental composition having been hypothesized (Cowgill et al., 2016; Cowgill, Niemi, Forte, & Trexler, 2018; Vincent et al., 2016; Vincent, Saintot, Mosar, Okay, & Nikishin, 2018). Structural shortening estimates (Trexler, 2018) and lower plate oroclinal bending estimates (van der Boon et al., 2018) indicating 230–280 km of shortening accommodated within the Greater Caucasus suggest that the Greater Caucasus basin was originally of comparable width (at minimum) to the extant Black Sea and Caspian Sea basins. Thus, an analogous basement, of thickness 8–20 km and composition similar to oceanic crust or mafic lower crust, is likely (Knapp et al., 2004; Mangino & Priestley, 1998; Nikishin et al., 2015).

The late Eocene to present history of the region reflects convergence of the Greater and Lesser Caucasus towards one another and closure of the intervening basin. Beginning in latest Eocene to earliest Oligocene time, the Greater Caucasus basin began to close by northward subduction/underthrusting, leading to the formation of the Greater Caucasus as a compressive orogen/accretionary prism (e.g. Adamia, Zakariadze, et al., 2011; Alizadeh et al., 2016; Cowgill et al., 2016; Dotduev, 1986; Forte, Cowgill, & Whipple, 2014; Gamkrelidze & Kakhadze, 1959; Kangarli et al., 2018; Khain, Gadjev, & Kengerli, 2007; Khain & Shardanov, 1960; Philip et al., 1989; Vincent, Morton, Carter, Gibbs, & Barabadze, 2007). The complete closure of the backarc basin(s) that separated the Lesser Caucasus from Eurasia was marked by the collision of the Lesser Caucasus arc terrane with the Greater Caucasus, the age of which is controversial (Cowgill et al., 2016; Cowgill et al., 2018; Vincent et al., 2016; Vincent et al., 2018). Burial histories suggest that flexural subsidence to the north of the Greater Caucasus was active during Late Miocene to Quaternary times, suggesting significant orogenic growth during that period (Ershov et al., 2003). Pro- and retro-wedge fold and thrust belts began to deform during Late Miocene time, with major deformation occurring in the Pliocene to Quaternary (Banks et al., 1997; Forte et al., 2013, 2014; Sobornov, 1994). Exhumation rates in the western Greater Caucasus increased by a factor of 10 around 7–5 Ma (Avdeev & Niemi, 2011; Vincent et al., 2020), coincident with slowing of Arabia–Eurasia convergence (Austermann & Iaffaldano, 2013) and kinematic reorganization of the Arabia–Eurasia plate boundary (Allen, Jackson, & Walker, 2004). These coinciding structural and kinematic changes have led to the hypothesis that collision began at ~5 Ma in the western Greater Caucasus and may have affected strain accommodation within the broader Arabia–Eurasia collision zone (Cowgill et al., 2016). An alternative hypothesis for the Eocene to

present evolution of the region is that collision between the Greater and Lesser Caucasus was largely complete by 34 Ma (Vincent et al., 2016). The provenance data presented here have implications for the timing of collision.

3.2 | Potential sources of Cenozoic foreland basin sediment

The Caucasus and surrounding regions contain three distinct domains of igneous and metamorphic basement and four distinct tectonostratigraphic sedimentary sequences that may have contributed sediment to the basin between the Greater and Lesser Caucasus during convergence and collision. Here, we outline these sources and their potential contribution to Caucasus Cenozoic foreland basin sediment.

Three distinct basement domains are potential sedimentary sources for Cenozoic Caucasus foreland basins: the Eurasian interior (consisting of the East European Craton and Urals), the Greater Caucasus basement and the Transcaucasus basement. The Archaean to Neoproterozoic crust of the East European Craton (Bogdanova et al., 2008) forms the core of the Eurasian interior at the longitude of the Caucasus and contributes sediment to rivers that drain into the Black and Caspian seas (Figure 2a; Allen et al., 2006; Wang, Campbell, Stepanov, Allen, & Burtsev, 2011). The East European Craton may also have contributed sediment to the Cenozoic foreland basin of the Caucasus (Allen et al., 2006). Some rivers that drain the East European Craton also include the Urals in their watershed, so sediment sourced from the Eurasian interior may also include detritus from the Palaeozoic Ural orogen (Allen et al., 2006). The second potential basement source is a predominantly late Palaeozoic (Hercynian) arc assemblage that constitutes the basement of the Greater Caucasus (Adamia, Zakariadze, et al., 2011; Somin, 2011). This arc assemblage is exposed in the core of the western portion of the Greater Caucasus (Figure 2b; Nalivkin, 1976). The third potential suite of basement sources is the isolated Precambrian to Palaeozoic massifs of the Transcaucasus and South Armenian Block, which together lie both between the Greater and Lesser Caucasus and within the Lesser Caucasus (the Dzirula, Khrami, Loki, and Dzarkuniatz massifs of the Transcaucasus are shown in Figure 2b; Aghamalyan, 1998; Gamkrelidze & Shengelia, 2007; Knipper & Khain, 1980; Mayringer, Treloar, Gerdes, Finger, & Shengelia, 2011; Nalivkin, 1976; Rolland et al., 2016; Zakariadze et al., 2007).

Four tectonostratigraphic sequences in the Caucasus may have contributed sediment to the Cenozoic foreland basin. The oldest sequence is Palaeozoic to Triassic in age and does not overlap the ages of the other, younger sequences. The Palaeozoic to Triassic sequence is marine and consists of shales, sandstones and carbonates that are locally found in depositional or structural contact with the Transcaucasus

basement and the southern margin of the Greater Caucasus basement (see reviews in Adamia et al., 1981; Khain, 1975; Şengör, Yılmaz, & Sungurlu, 1984). Exposures of this sequence immediately to the south of the Greater Caucasus basement are called the Dizi Series (Adamia, Zakariadze, et al., 2011; Somin, 2011; Vasey et al., 2020). Palaeozoic to Triassic sedimentary rocks are exposed over only a minor area within the Caucasus.

The three tectonostratigraphic sequences that constitute the vast majority of exposed bedrock in the Caucasus are contemporaneous sequences of predominantly Jurassic to Cretaceous strata that are markedly different in composition and sedimentology. These three sequences, which we describe here in order of exposure from south to north, are thought to have been deposited on the flanks of the Lesser Caucasus arc and in the Greater Caucasus basin (e.g. Nalivkin, 1976; Rolland et al., 2011; Saintot, Brunet, et al., 2006; Sosson et al., 2010; Vincent et al., 2016; Zonenshain & Le Pichon, 1986). The southernmost of the three sequences, the Jurassic to Eocene Lesser Caucasus arc sequence is exposed in the Lesser Caucasus and includes calc-alkaline volcanic, volcanoclastic and carbonate strata intruded by Jurassic to Eocene plutons that reflect volcanic arc activity in the Lesser Caucasus (Figure 2b; Kopp & Shcherba, 1985; Nalivkin, 1976; Rolland et al., 2011; Sosson et al., 2010; Sahakyan et al., 2017). Exposed on the southern slope of the Greater Caucasus is the Jurassic to Cretaceous Greater Caucasus volcanoclastic sequence, which includes a thick sequence of mafic to intermediate volcanic and volcanoclastic strata and carbonates with local Jurassic intrusions (Figure 2b; Kopp, 1985; Mengel et al., 1987; Nalivkin, 1976). The Greater Caucasus volcanoclastic sequence is thought to have been deposited in the Greater Caucasus basin (e.g. Vincent et al., 2016). Within the Greater Caucasus, to the north of the volcanoclastic sequence, is a Jurassic to Cretaceous sequence dominated by marine sandstones and shales (Figure 2b; e.g. Bochud, 2011; Saintot, Brunet, et al., 2006; Vincent, Morton, Hyden, & Fanning, 2013). We term this sequence the Greater Caucasus siliciclastic sequence in order to differentiate it from the Greater Caucasus volcanoclastic sequence, although some carbonates are present. The sedimentary architecture of the Greater Caucasus siliciclastic sequence, inferred from seismic data, suggests the sequence is derived from north of the Greater Caucasus (Sholpo, 1978). Because the Lesser Caucasus arc sequence, Greater Caucasus volcanoclastic sequence and Greater Caucasus siliciclastic sequence together account for the majority of exposed bedrock in the Caucasus today (Figure 2b), they are anticipated to have been significant sources for Oligocene to Quaternary foreland basin sedimentation.

4 | METHODS

We report 29 new detrital zircon U-Pb age samples (Table S1) from Cenozoic sandstones and modern river sands

comprising 7,090 total ages (Table S2). Mineral separation was conducted at the University of Michigan. Heavy mineral fractions were mounted in epoxy and polished to expose crystal interiors. Mounts were made of entire heavy mineral fractions, rather than hand selected individual zircon grains, in order to ensure that representative random samples of zircon were analysed. Mount imaging was conducted at the University of Michigan and the University of Arizona Laserchron Center. U-Pb analyses were conducted at the University of Arizona Laserchron Center using a laser ablation system attached to a Thermo Element 2 single collector ICP-MS (Gehrels, Valencia, & Ruiz, 2008; Pullen, Ibáñez-Mejía, Gehrels, Ibáñez-Mejía, & Pecha, 2014). Analyses >20% discordant are excluded from further interpretation. Where practical, we analysed at least 300 zircon grains per sample, which provides more robust characterization of zircon age signatures than analyses with typical ($n \sim 100$) sample sizes (Pullen et al., 2014).

4.1 | Sampling

Understanding provenance changes during the evolution of an orogen (Figure 1) requires characterizing the zircon age signature of potential source areas and characterizing the contribution of those sources to foreland basin deposits. We use 16 new samples of modern river sands from targeted catchments that contain specific bedrock ages and lithologic types, along with published modern and bedrock detrital zircon samples (Allen et al., 2006; Cowgill et al., 2016; Vasey et al., 2020; Wang et al., 2011), to characterize the zircon age signatures of the potential source areas (Figures 3–5), as described in the previous section. Using modern river sand samples to characterize potential sources is an efficient way to capture well-mixed, representative zircon age signals associated with erosion from the source area (Figure 3). This method assumes that present exposures are representative of those that contributed sediment earlier in the Cenozoic (e.g. the Jurassic sandstones presently exposed in the range yield the same detrital zircon age distribution as Jurassic sandstones exposed in the Cenozoic), which we view as realistic given the age ranges of exposed bedrock and the structural style of the Caucasus.

In order to understand the changing sources of foreland basin sediment over time, we compare the zircon age signatures of potential sources to the zircon age distributions of Cenozoic foreland basin rock samples (Figure 3). We report 13 new samples taken from different stratal levels of three Cenozoic foreland basin sections (western, central and eastern sections) located on the southern margin of the Greater Caucasus (Figures 4–6). Five new samples were analysed from the western foreland basin section from rocks of

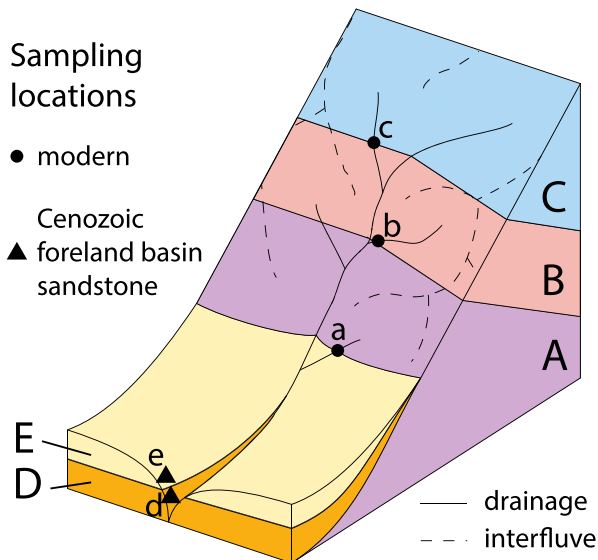


FIGURE 3 We use a two part detrital zircon sampling strategy to understand the evolution of foreland basin sediment provenance. We collect samples of foreland basin strata (rock samples d and e, of foreland basin units D, E), and we use modern samples of targeted catchments to characterize potential sources contributing to the sampled foreland strata (river sands at locations a, b and c provide detrital zircon age signatures of units A, B and C respectively).

Oligocene to Quaternary age (Figure 5b). Two samples were analysed from the central foreland basin section of Middle Miocene and Late Miocene age (Figure 5a). Six samples

were analysed from the eastern foreland basin section, including rocks of Cretaceous–Palaeocene to Pliocene age (Figure 5c). In addition to these new samples, our analyses are integrated with five foreland basin samples from the western Greater Caucasus (Vincent et al., 2013) and four samples from a Pliocene section at the far eastern extent of the Greater Caucasus (Allen et al., 2006).

4.2 | Data visualization

Throughout the paper, samples are coloured by comparison to three endmember samples using the Bayesian Population Correlation (BPC) metric (Tye, Wolf, & Niemi, 2019). BPC values range from 0 to 1 based on the likelihood that two sampled populations are the same versus different, with values closer to 1 indicating greater population correspondence (Tye et al., 2019). The three endmember samples were chosen because they highlight first order age distinctions among the potential sources: the Eurasian interior (represented by sample Volga; Wang et al., 2011) is dominated by Proterozoic zircon ages, the Greater Caucasus (represented by sample EGC-4) contains predominantly Palaeozoic zircon ages (Adamia, Zakariadze, et al., 2011; Somin, 2011), and the Lesser Caucasus (represented by LC-3) is characterized by Jurassic to Eocene zircon ages (e.g. Sosson et al., 2010).

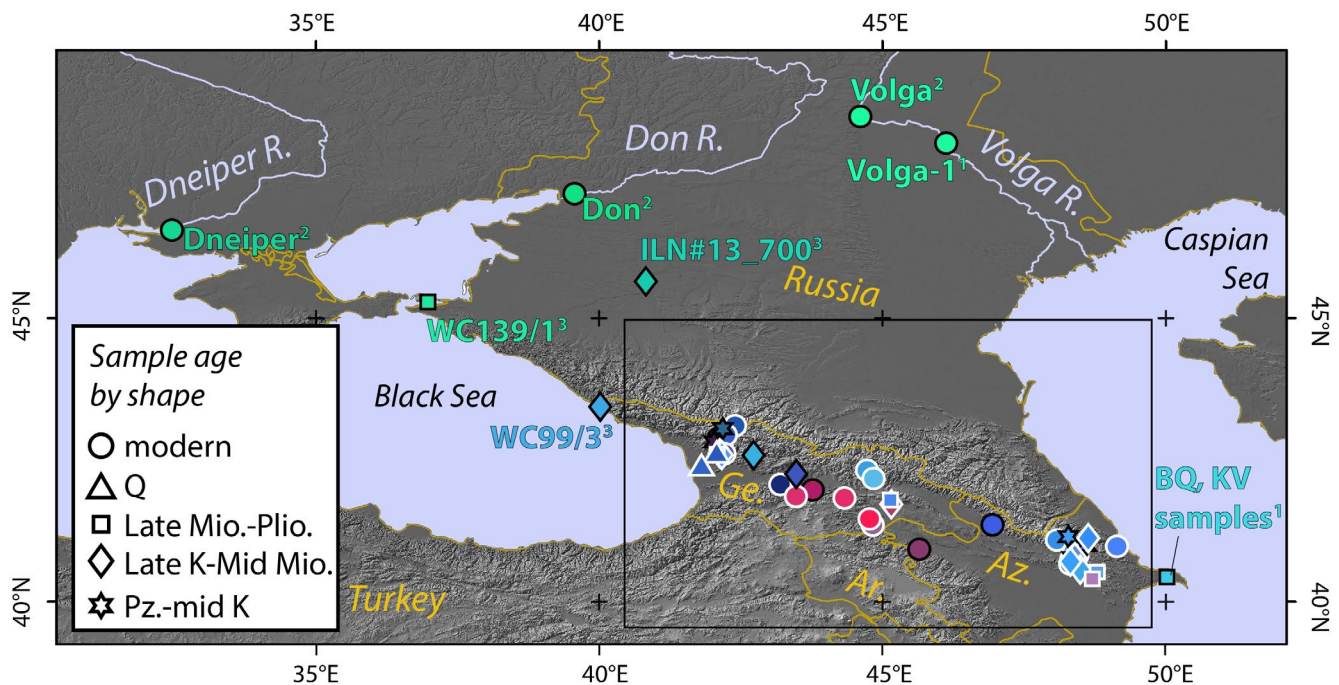


FIGURE 4 New and published sampling covers the Eurasian interior, the Greater Caucasus and the Lesser Caucasus. Sample colours indicate affinity to the Eurasian interior (green), the Greater Caucasus (blue) or the Lesser Caucasus (red); see Figure 7 and Section 4.2 for details. Symbol outlines are white for new samples and black for previously published samples. Black rectangle shows the extent of Figure 5a. Samples outside this rectangle have their names displayed and are superscripted according to source publication: 1–Allen et al. (2006); 2–Wang et al. (2011); 3–Vincent et al. (2013). Samples inside the rectangle have their names displayed in Figure 5. Abbreviations for geologic time are as follows: Pz–Palaeozoic, K–Cretaceous, Mio–Miocene, Plio–Pliocene, Q–Quaternary.

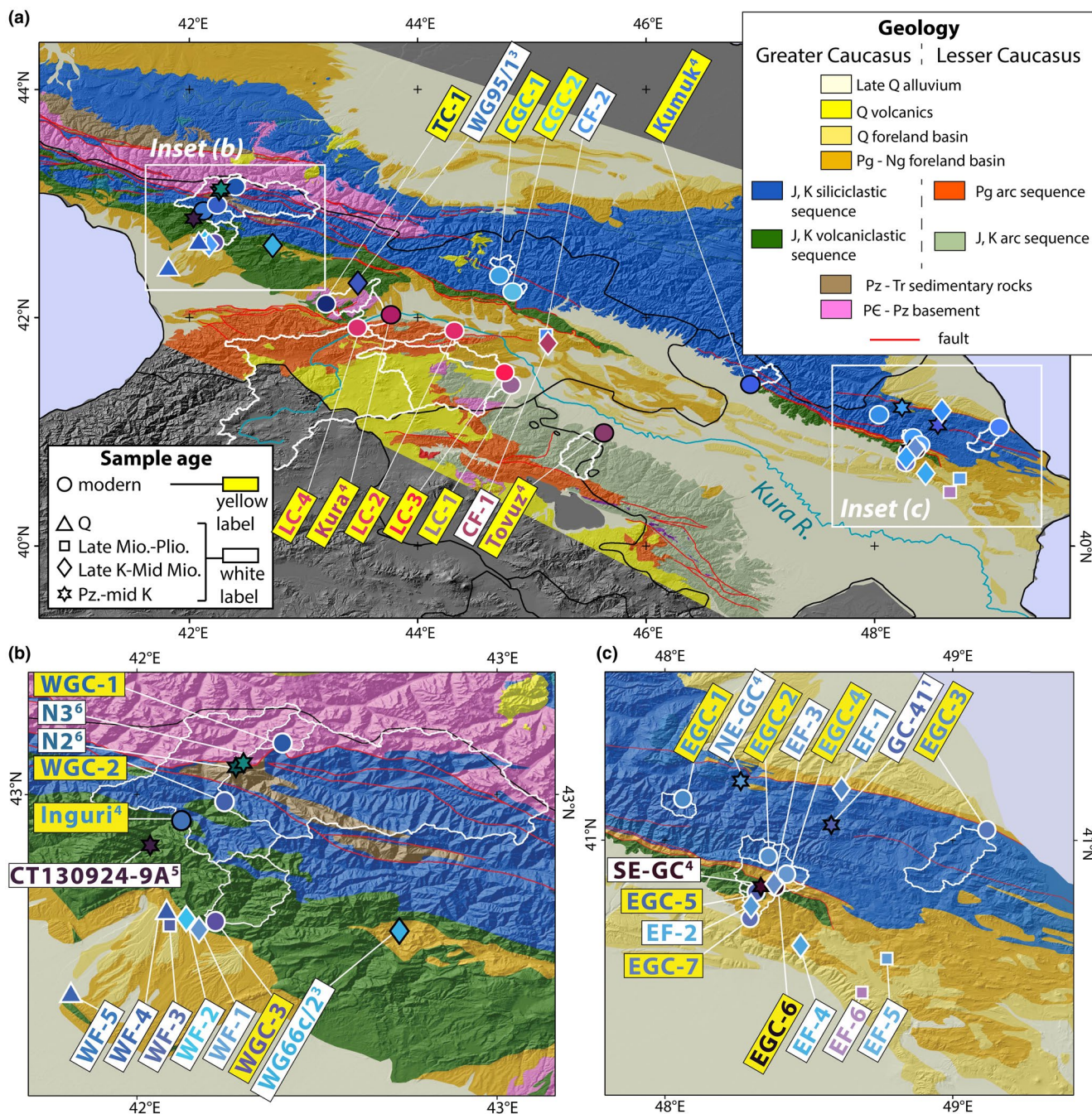


FIGURE 5 Simplified geology and detrital zircon sample locations in the Greater and Lesser Caucasus. Sample names are shown in rectangles and sample colours are as in Figure 4. Political boundaries are shown in black and catchment boundaries of modern samples are shown in white. Abbreviations for geologic time are as follows: PC–Precambrian, Pz–Palaeozoic, Tr–Triassic, J–Jurassic, K–Cretaceous, Pg–Palaeogene, Ng–Neogene, Mio–Miocene, Plio–Pliocene, Q–Quaternary. For samples not from this study, sample name superscripts reflect source publication as in Figure 4 with three additions: 4–Cowgill et al. (2016), 5–Trexler (2018), 6–Vasey et al. (2020).

These three endmembers were chosen because they are broadly representative of samples from their respective source areas and because they have large sample sizes ($n \sim 300$), where available. The colouring scheme works as follows: each sample is assigned an RGB triplet where the

red value is equal to the BPC value of the sample compared to the Lesser Caucasus endmember, the green value comes from comparison to the Eurasian interior endmember and the blue value comes from comparison to the Greater Caucasus endmember (Figure 7).

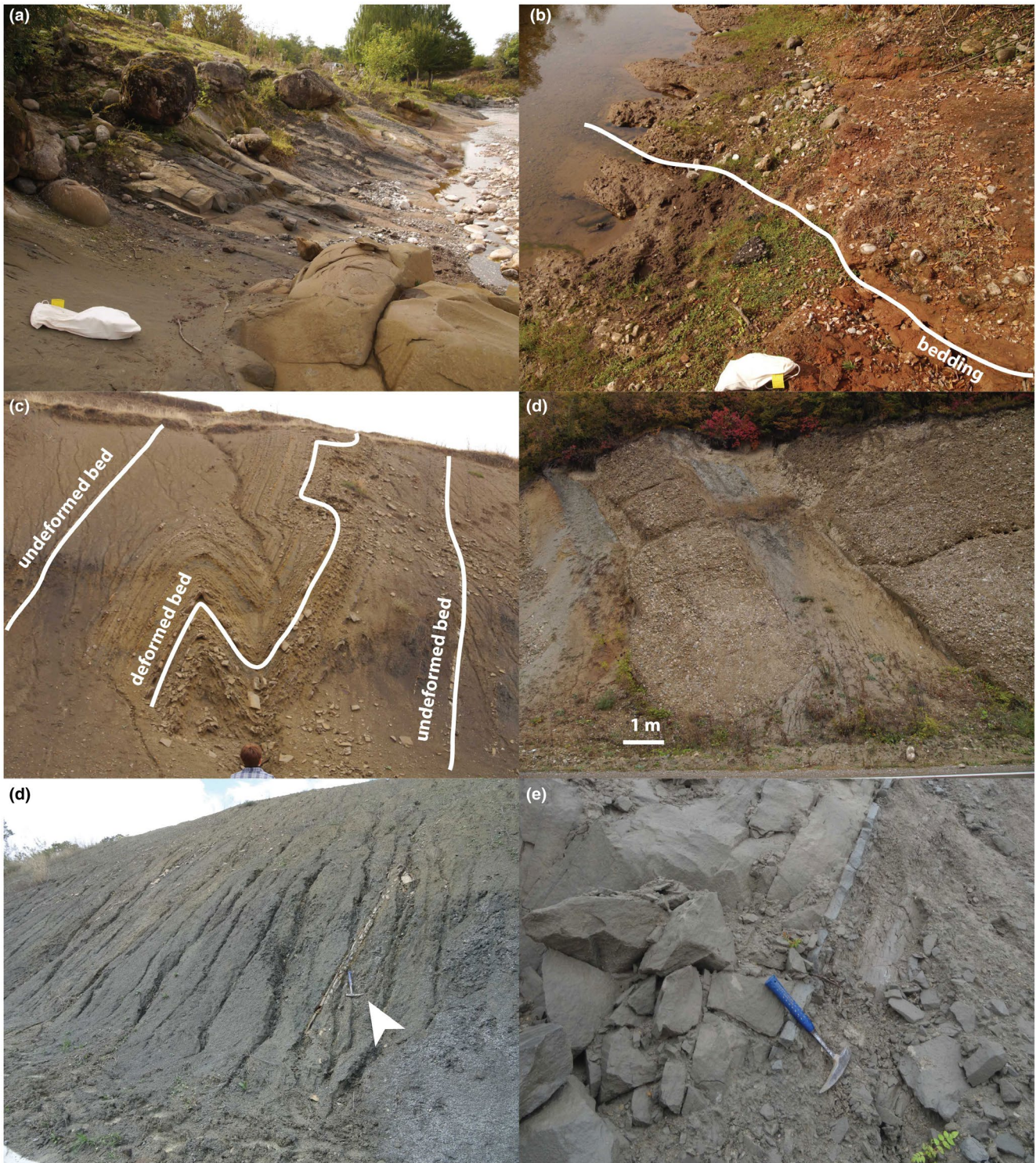
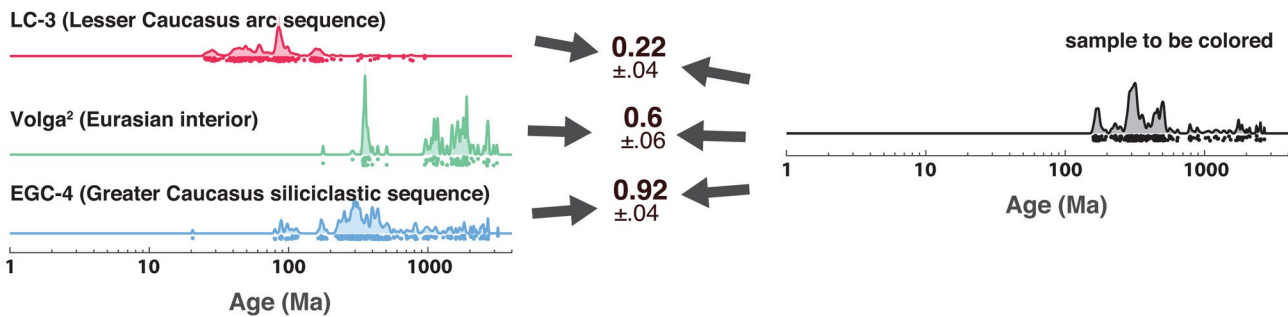


FIGURE 6 Photographs of sampled Cenozoic foreland basin strata. (a) Oligocene, Early Miocene, or Middle Miocene sandstones and organic-rich shales of the western foreland basin section (sample WF-2). (b) Latest Pliocene conglomerate of western section, bedding marked in white (sample WF-3). (c) Middle Miocene organic-rich sandstone-shale sequence of the central section with bedding of undeformed and deformed horizons marked in white (sample CF-1). (d) Late Miocene conglomerate of the central section (sample CF-2). (e) Oligocene or Early Miocene sandstone and shale of the eastern section with arrow indicating rock hammer for scale (sample EF-4). (f) Pliocene sandstone of the eastern section (sample EF-6).

(a) BPC calculated relative to endmembers



(b) BPC values used as R, G, B values to color sample

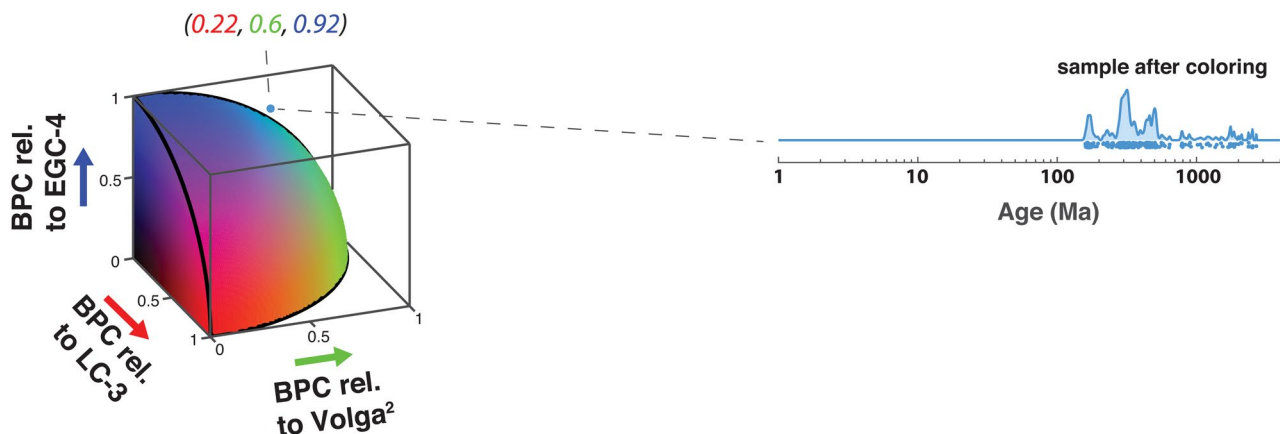


FIGURE 7 Throughout this paper, samples are coloured according to their BPC value (Tye et al., 2019) relative to three representative endmembers of the Eurasian interior, Greater Caucasus, and Lesser Caucasus. (a) BPC values are calculated between each sample and the three endmember samples. (b) Calculated BPC values are used as R, G, B values for colouring each sample. The coloured surface shown is a visual aid; samples do not need to fall on this surface.

5 | SOURCE AREA DETRITAL ZIRCON SIGNATURES

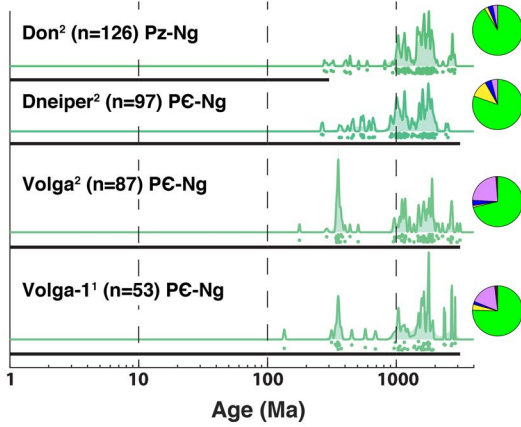
5.1 | Detrital zircon age signatures of potential sources for Caucasus Cenozoic sediment

In order to use detrital zircon data from foreland basin deposits to understand the Cenozoic tectonic history of the Caucasus, we must first characterize the zircon age signatures of potential sediment sources for the foreland basin deposits. In this section, we discuss the zircon age distributions that distinguish seven potential sources (Figures 8, S1) that outcrop within the Caucasus and surrounding region (Figures 4 and 5). Three of these sources are regional basement domains (the Eurasian interior, the Greater Caucasus basement, and the Transcaucasus basement). One potential source suite is the pre-Jurassic sedimentary sequences that crop out over small areas adjacent to Greater Caucasus and Transcaucasus basement outcrops. Three sources are Jurassic to Eocene tectonostratigraphic sequences (the Lesser Caucasus arc, Greater

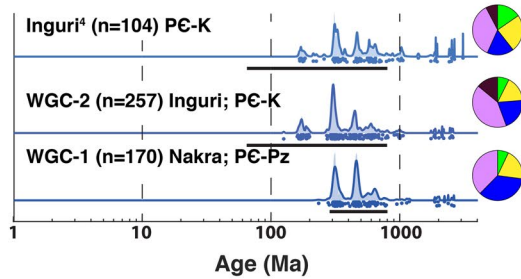
Caucasus siliciclastic, and Greater Caucasus volcanoclastic sequences). We first discuss the basement domain sources.

Three distinct basement domain sources can be distinguished by their detrital zircon age signatures: the Eurasian interior (includes the East European Craton and Urals; Figures 8a, S1a), the crystalline basement exposed in the Greater Caucasus (Figures 8b, S1b), and the basement massifs of the Transcaucasus (Figures 8c, S1c). Modern samples from rivers that drain the Eurasian interior contain at least 70% zircon ages >900 Ma, which are associated with the East European craton (Figure 8a; Allen et al., 2006; Bogdanova et al., 2008). Some samples representing the Eurasian interior also contain a subordinate peak at ~360 Ma derived from the Urals (Allen et al., 2006). Rivers that drain the Eurasian interior contain very few Mesozoic zircon grains and no Cenozoic zircon grains. Detritus of the Greater Caucasus basement (Figure 8b) is primarily identifiable by concentrated age peaks centred on 300 Ma and 450 Ma. Scattered Neoproterozoic to Middle Palaeozoic ages are also present in the Greater Caucasus basement rocks, defining a broad age peak centred on 600 Ma (Figure 8b). Transcaucasus basement massifs are targeted

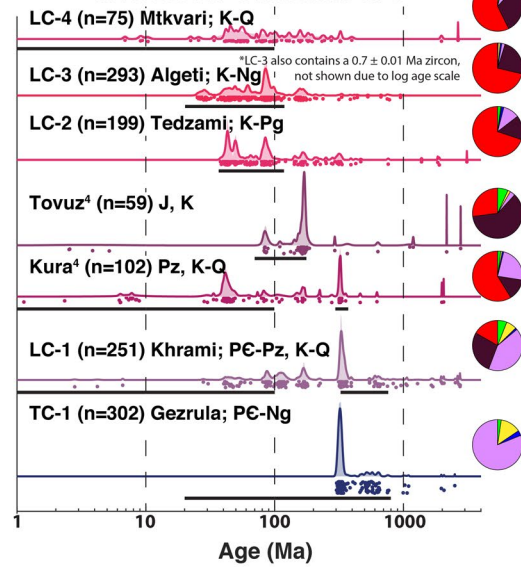
(a) Eurasian interior



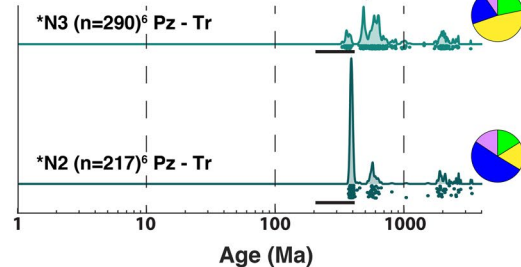
(b) Greater Caucasus basement



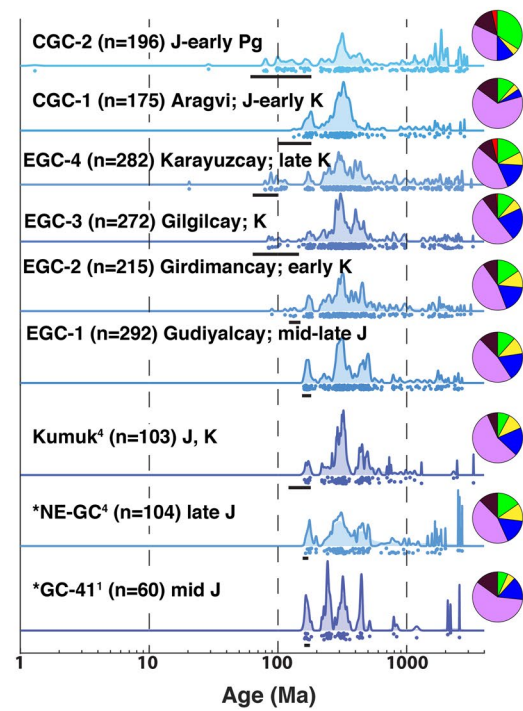
(c) Transcaucasus basement and Lesser Caucasus arc



(d) Pre-Jurassic sedimentary rocks



(e) Greater Caucasus siliciclastics



(f) Greater Caucasus volcanoclastics

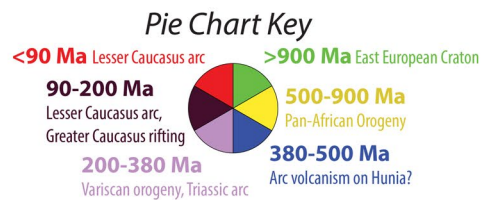
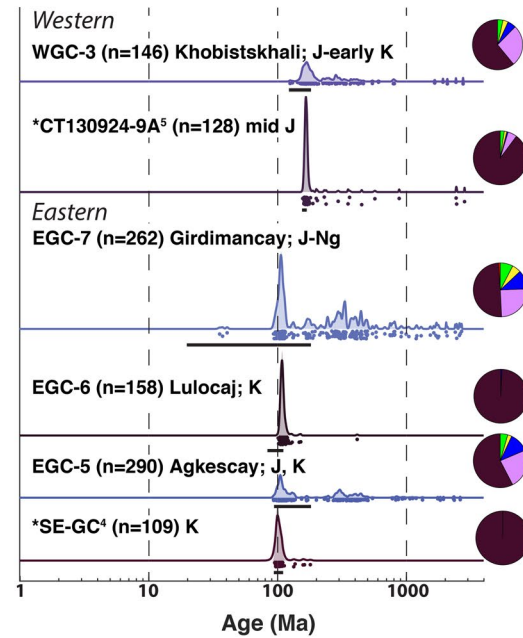


FIGURE 8 Detrital zircon age signatures from targeted modern river samples from (a) the Eurasian interior, (b) the Greater Caucasus basement, (c) the Transcaucasus basement and Lesser Caucasus arc sequence, (d) pre-Jurassic sedimentary rocks, (e) the Greater Caucasus siliciclastic sequence and (f) the Greater Caucasus volcanoclastic sequence. Published modern river and bedrock samples from these sources are also shown (bedrock samples are marked with an asterisk *). Each sample is labelled with the sample name, sample size, name of modern river sampled (if applicable/available) and its age or the ages of strata within the sampled catchment (Asch, 2005; Nalivkin, 1976). The plot of each sample shows a probability density plot (Hurford, Fitch, & Clarke, 1984) as a solid line, a kernel density estimate (Shimazaki & Shinomoto, 2010; Silverman, 1986; Vermeesch, 2012) as a shaded area, age observations ignoring analytical uncertainty as a band of dots beneath the curves (vertical scatter for visual clarity), and a black bar that shows the age of the sample (for bedrock samples) or the ages of bedrock strata within the sampled catchment (for modern samples). A pie chart of ages is shown to the right of each sample, as outlined in the key (see Section 7 for interpretation of ages). Previously published samples are marked with a superscript, corresponding to references as in Figures 4 and 5. Age abbreviations are as Figure 5. The Greater Caucasus volcanoclastic sequence is subdivided into a western and eastern portion, with the western portion largely consisting of Jurassic strata and the eastern portion consisting largely of Cretaceous strata. Samples are coloured as shown in Figure 7, and are arranged by region. Empirical cumulative distribution functions of these samples are shown in Figure S1.

by sample TC-1 and are also included in the catchments of samples LC-1 and Kura (Figures 5a; 8c). Pre-Mesozoic ages in these samples are dominated by a single peak at ~300 Ma (Figure 8c). Samples derived from Transcaucasus basement massifs also contain scattered Neoproterozoic to Palaeozoic ages that define a broad peak near 600 Ma (Figure 8c). The distinguishing detrital zircon age characteristics of the three basement domain sources are that the Eurasian interior is the only source of abundant zircon ages >900 Ma, the Greater Caucasus basement contains large, subequal zircon age peaks at ~300 Ma and ~450 Ma, and the Transcaucasus basement massifs contain only one major age peak, at ~300 Ma (Table 1).

One potential sediment source in the Caucasus is a set of Late Palaeozoic to Triassic, fine-grained clastic to carbonate sedimentary successions exposed over small areas adjacent to the Greater Caucasus basement and Transcaucasus basement massifs (Figures 5b, 8d, S1d; Adamia, Zakariadze, et al., 2011; Khain, 1975; Şengör et al., 1984; Vasey et al., 2020). One of these successions, the Dizi Series, is located directly to the south of the Greater Caucasus basement (Figure 8d; Adamia, Zakariadze, et al., 2011; Khain, 1975; Şengör et al., 1984). Detrital zircon age spectra from the Dizi Series are characterized by an age peak between ~500 and 800 Ma, scattered Archaean to Palaeoproterozoic ages, and in one case, a 380 Ma age peak that accounts for >60% of measured ages (Figure 8d; samples N2 and N3; Vasey et al., 2020). The detrital zircon U-Pb age signatures of samples N2 and N3, two bedrock samples from the Dizi Series, differ markedly from modern samples that include the Dizi Series and other Palaeozoic to Triassic successions within their source catchments (see samples Inguri, WGC-2, and LC-1; Figures 5 and 8), suggesting the signatures of samples N2 and N3 are not effectively propagated through the sedimentary system. In addition, the signatures of N2 and N3 are different from all foreland basin samples, as we later show. The lack of propagation of the Dizi Series age signatures is likely due to the fine-grained clastic and carbonate strata that dominate Palaeozoic to Triassic sedimentary sequences on the southern

slope of the Greater Caucasus and within the Transcaucasus/Lesser Caucasus (Adamia, Zakariadze, et al., 2011; Khain, 1975), and may also be due to the small exposure area of these successions compared to other potential sedimentary sources in the Caucasus (Figure 5). Because the detrital zircon age signatures of samples N2 and N3 appear not to be effectively propagated through the sedimentary system, it is not possible to use detrital zircon ages to determine whether the pre-Jurassic sequences they represent contributed sediment to the Cenozoic foreland basin.

The final three sources we characterize are three Jurassic to Eocene tectonostratigraphic packages that outcrop over large areas in the Caucasus region (Figure 5): the Lesser Caucasus arc sequence (Figures 8c, S1c), Greater Caucasus siliciclastic sequence (Figures 8e, S1e) and Greater Caucasus volcanoclastic sequence (Figures 8f, S1f). Samples derived from the Lesser Caucasus arc sequence can be recognized by the ubiquity of zircon ages 90 Ma and younger (Figure 8c), which are virtually absent in other potential sources. Lesser Caucasus arc sequence samples also contain an age peak centred on 170 Ma. Samples of the Greater Caucasus siliciclastic sequence (Figure 8e) share two major zircon age peaks with the Greater Caucasus basement (~300 Ma and ~450 Ma), though in the Greater Caucasus siliciclastic sequence these age peaks are wider than in the Greater Caucasus basement. Discordance does not appear to be systematically greater in Greater Caucasus siliciclastic sequence samples than in Greater Caucasus basement samples (Figure S3), so the increased scatter in the ~300 Ma and ~450 Ma age peaks in the Greater Caucasus siliciclastic samples is likely to truly reflect age scatter in the source area for the Greater Caucasus siliciclastic sequence. Additional age populations present in some or all Greater Caucasus siliciclastic sequence samples include Permian to Triassic ages, either on the margin of a ~300 Ma peak or as a separate peak; a ~170 Ma zircon age peak; scattered Precambrian to Palaeozoic ages ranging from 3 Ga to 500 Ma; and small quantities of ~100 Ma zircon ages (Figure 8e). The Greater Caucasus volcanoclastic sequence yields

TABLE 1 Diagnostic detrital zircon age signatures of potential sources of Cenozoic foreland basin strata in the Caucasus

Potential source	Map Unit(s)	Notable age peaks	Notes
Eurasian interior	None (Eurasian interior is north of map area)	>900 Ma	Likely ultimate source for most ages >900 Ma in study area
Greater Caucasus basement	PC–Pz basement (Greater Caucasus)	300 Ma, 450 Ma	300 Ma, 450 Ma age peaks subequal, narrow
Transcaucasus basement	PC–Pz basement (south of Greater Caucasus)	300 Ma	no peak at 450 Ma
Palaeozoic to Triassic sedimentary sequences	Pz–Tr sedimentary rocks	500–800 Ma, 380 Ma	Not a significant contributor to foreland samples
Lesser Caucasus arc sequence	J, K arc sequence; Pg arc sequence	<90 Ma, 170 Ma	Likely ultimate source for most ages <90 Ma in study area
Greater Caucasus siliciclastic sequence	J, K siliciclastic sequence	300 Ma, 450 Ma	Age peaks wide with scattered ages throughout Palaeozoic
Greater Caucasus volcanoclastic sequences	J, K volcanoclastic sequence	170 Ma or 105 Ma	Unimodal

Note: Map Unit(s) column shows corresponding units on Figure 5.

largely unimodal detrital zircon age samples, which are centred on 170 Ma in the western Greater Caucasus and 105 Ma in the eastern Greater Caucasus (Figure 8f). Samples that represent the Greater Caucasus volcanoclastic sequence and that also contain appreciable quantities of other age peaks (samples WGC-3, EGC-5, EGC-7) come from catchments that include both Greater Caucasus volcanoclastic strata and Greater Caucasus siliciclastic strata. Detrital zircon age signatures of the three Jurassic to Eocene tectonostratigraphic sequences in the Caucasus can be distinguished by the fact that the Lesser Caucasus arc sequence contains plentiful zircon ages <90 Ma, the Greater Caucasus siliciclastic sequence contains wide age peaks centred on 300 and 450 Ma, and the Greater Caucasus volcanoclastic sequence yields unimodal zircon U-Pb age peaks at 170 and 105 Ma (Table 1).

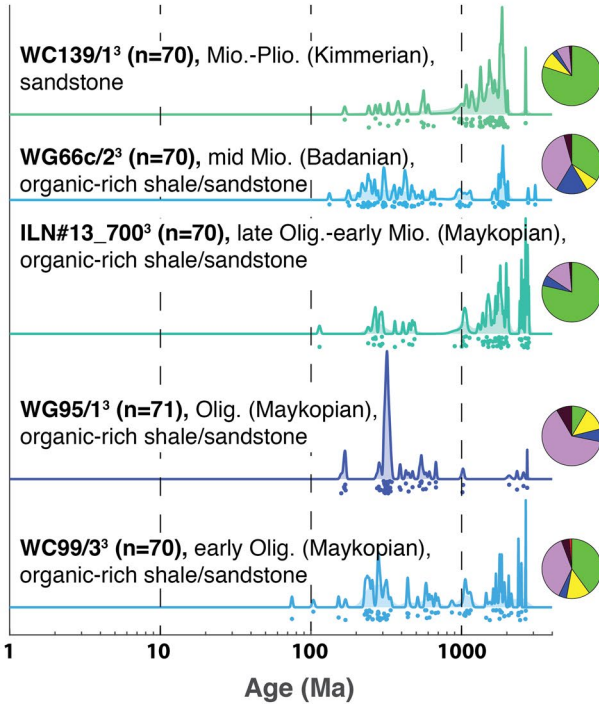
The zircon age signature characteristics described above permit the discrimination of six different potential sources for Caucasus foreland basin sediment (Table 1). These sources include the Eurasian interior, Greater Caucasus basement, Transcaucasus basement, the Lesser Caucasus arc sequence, the Greater Caucasus siliciclastic sequence and the Greater Caucasus volcanoclastic sequences. Because these sources have distinct detrital zircon U-Pb age spectra, their unique provenance signatures can be distinguished in foreland basin stratigraphic sequences.

6 | FORELAND BASIN ZIRCON U-Pb CHARACTERISTICS AND PROVENANCE INTERPRETATION

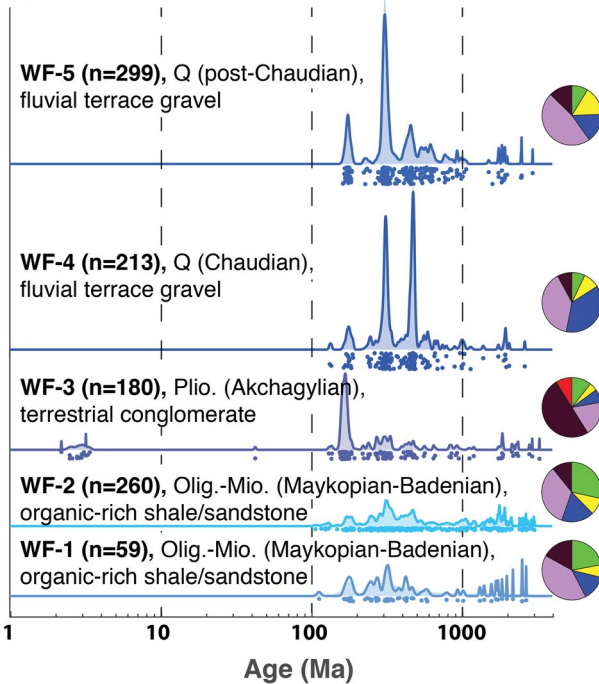
We use detrital zircon U-Pb age distributions from foreland basin sedimentary sections, in combination with the source

signatures outlined above, to infer which sources contributed sediment to the foreland basin and changes in provenance over time. Here, we describe the zircon age distributions of new and previously published samples from foreland basin sedimentary strata deposited during Cenozoic time in the basin between the Greater and Lesser Caucasus (Figures 9, S2). In describing these age distributions, we discuss sample composition and sedimentology (Figure 6 shows photos of selected sampled lithologies) and the stratigraphic context of the samples (Figure 10). We also compare foreland basin zircon age signatures with both the sources discussed above and published data sets and discuss the implications for source exposure and sediment routing systems. New foreland samples were collected from three sedimentary sections (western, central, and eastern) that were deposited in Palaeogene to Quaternary time (Figures 5 and 9). We also discuss published samples from a Pliocene section at the far eastern extent of the range (Allen et al., 2006), as well as a set of previously published samples that are distributed over a wide area of the western Greater Caucasus (Vincent et al., 2013). Age constraints for our samples are based on published geologic mapping (Dzhanelidze & Kandelaki, 1957; Edilashvili, 1957; Gamkrelidze & Kakhadze, 1959; Khain & Shardanov, 1960; Mekhtiev, Gorin, Agabekov, & Voronin, 1962; Nalivkin, 1976; Voronin, Gavrillov, & Khain, 1959) unless otherwise noted, and published age constraints are used for previously published samples. The zircon age distributions are discussed roughly in order from west to east, beginning with the previously published distributed samples in the western portion of the range (Vincent et al., 2013) and proceeding with our new western, central, and eastern sampled sections, followed by the published far eastern section (Allen et al., 2006, Figure 9).

(a) *Distributed western samples*
(Vincent et al., 2013)



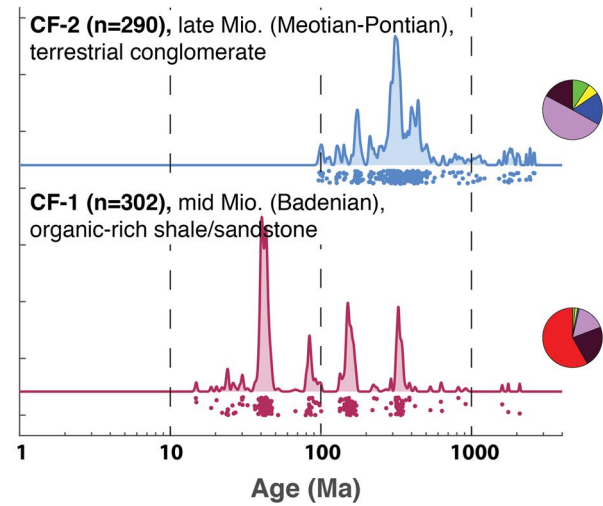
(b) *Western section*



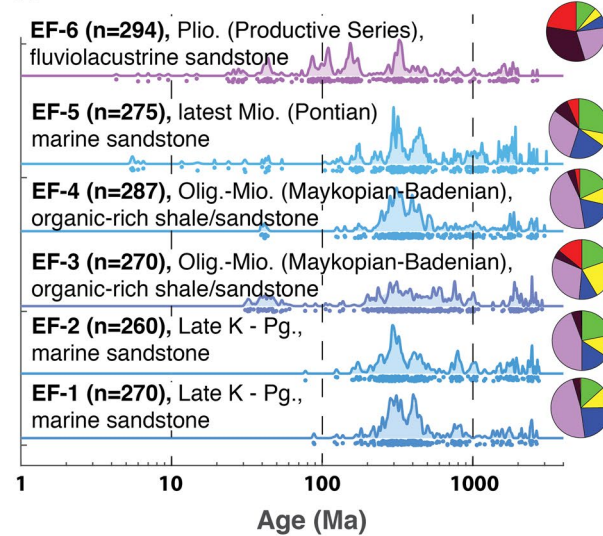
Pie Chart Key



(c) *Central section*



(d) *Eastern section*



(e) *Far eastern section*
(Allen et al., 2006)

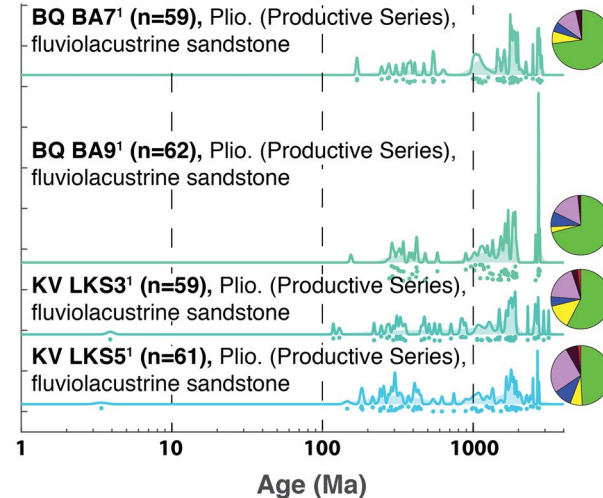


FIGURE 9 Detrital zircon age spectra of foreland basin sedimentary rocks reflect Cenozoic provenance variation over space and time. Previously published samples from distributed locations in the western Greater Caucasus are shown (a; Vincent et al., 2013). New samples were collected from western (b), central (c) and eastern (d) foreland basin sections. Previously published samples from a Pliocene section at the far eastern extent of the range are also reported (e; Allen et al., 2006). Spectra are shown in reverse stratigraphic order in each panel. Symbology is the same as Figure 8. Sample ages, with regional stage in parentheses, and rock types, are listed. Abbreviations are as in previous figures, plus: Olig.–Oligocene, Mio.–Miocene, Plio.–Pliocene, Pleis.–Pleistocene. Empirical cumulative distribution functions of these samples are shown in Figure S2.

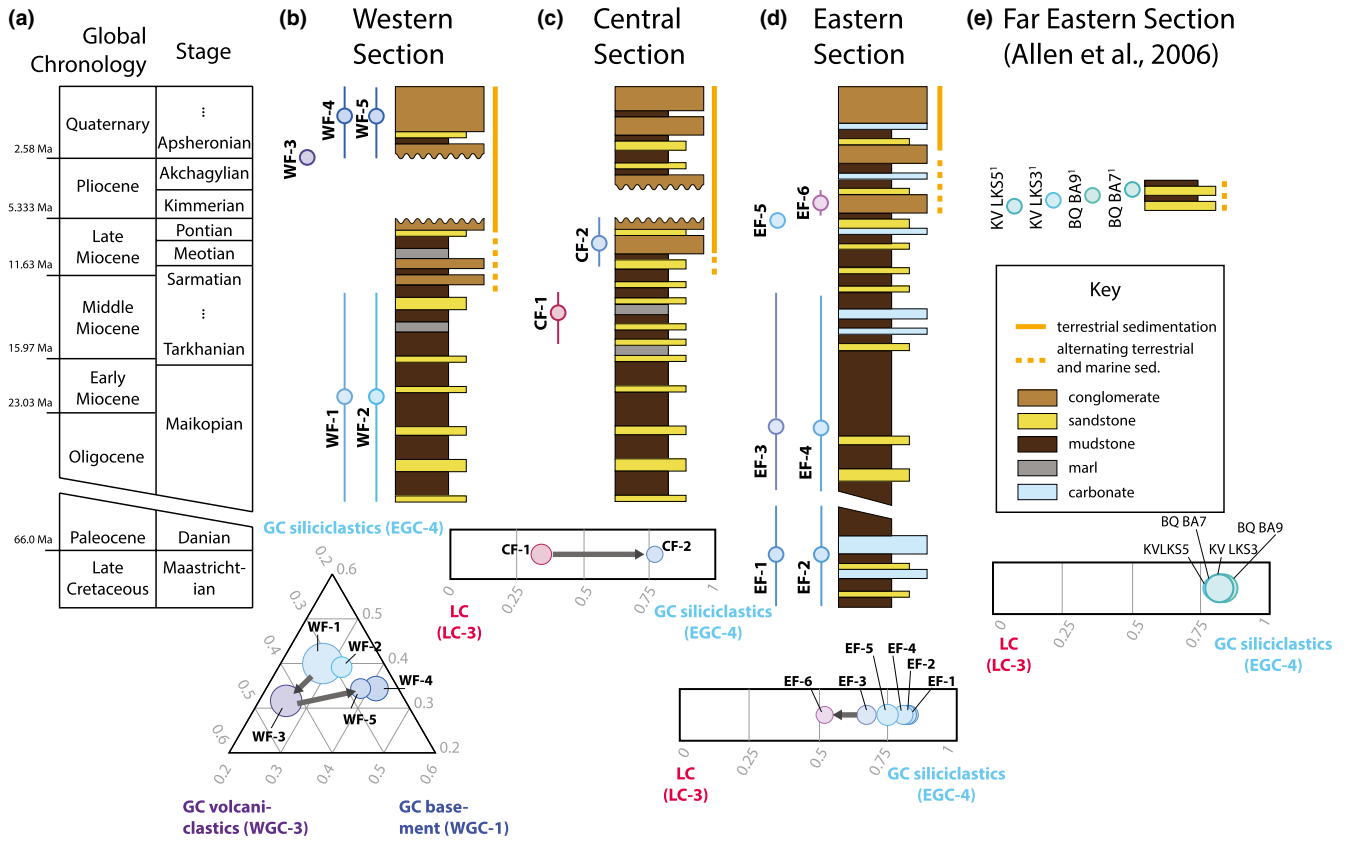


FIGURE 10 Foreland basin samples are shown in stratigraphic context. (a) Global chronology with stratigraphic stage names (Paratethyan stage names are used for the Neogene; Jones & Simmons, 1997). (b–e) western, central, eastern, and far eastern sampled foreland basin sections. Sample ages are depicted with symbols next to each stratigraphic column, with error bars representing the range of possible ages. Symbols are coloured using the BPC colouring scheme used throughout this paper (Figure 7). Beneath each section is a plot of normalized BPC of the samples relative to potential sources for the section (source sample numbers shown in parentheses), with arrows indicating trends over time (see Tables S3, S4 for BPC results). The endmembers for each plot are chosen based on which endmember sources (Figure 8) are inferred to have contributed detrital zircon grains to each section (see text for further discussion). Plot symbol size is mean BPC uncertainty (1σ) with respect to the endmember samples, and symbols for the central and eastern sections have been doubled in size for visual clarity. Sources from the Greater and Lesser Caucasus are abbreviated GC and LC respectively. Stratigraphy is schematic, based on Edilashvili (1957), Dzhaneldidze and Kandelaki (1957), Gamkrelidze and Kakhazdze (1959), Voronin et al. (1959), Khain and Shardanov (1960), Mekhtiev et al. (1962), Hinds et al. (2004), Vincent et al. (2014) and field observations. Blank space in sections marks missing time due to unconformities. Unconformities without significant missing time are not shown. The distributed western samples of Vincent et al. (2013) are not depicted stratigraphically because they are from a variety of locations with variable stratigraphy

6.1 | Distributed foreland basin samples of the western Greater Caucasus

Previously published Cenozoic samples from the western Greater Caucasus include five samples from early Oligocene to latest Miocene/earliest Pliocene time (Figures 9a, S2a; Vincent et al., 2013). This group of five samples

includes two samples that lie to the north-west of the Greater Caucasus (samples ILN#13_700 and WC139/1; Figure 4), and three samples located on the southern margin of the range (samples WC99/3, WG66c/2, and WG95/1; Figures 4 and 5). The two samples north-west of the Greater Caucasus, late Oligocene to early Miocene sample ILN#13_700 and Miocene to Pliocene sample WC139/1, are composed mostly

of zircon grains >900 Ma (Figure 9a) with some scattered Neoproterozoic and Palaeozoic ages. Overall these two samples show a clear affinity to the Eurasian interior (Figure 8a). Early Oligocene sample WC99/3, an Oligocene marine sandstone sample from the south side of the westernmost Greater Caucasus, contains ~40% zircon ages >900 Ma, as well as a 230–360 Ma age peak (Figure 9a). This sample shows a partial affinity to the Eurasian interior, with the 230–360 Ma age peak suggesting a partial affinity to the Greater Caucasus siliciclastic sequence. Middle Miocene marine sandstone sample WG66c/2 was collected from near our western section (Figure 5b), and contains scattered Palaeozoic to Triassic ages that coalesce around two broad age peaks at 450 and 300 Ma, as well as ~35% ages >900 Ma (Figure 8a). These ages indicate that WG66c/2 was likely derived predominantly from the Greater Caucasus siliciclastic sequence. Sample WG95/1 was collected from an Oligocene sandstone in close proximity to the Dzirula Massif (Figure 5a), a Transcaucasus basement massif, and has a detrital zircon age distribution dominated by a narrow ~300 Ma age peak (Figure 9a) that closely matches that of modern detritus from the Dzirula Massif (sample TC-1, Figure 8b).

The spatial distribution of source affinities within these samples has implications for the Cenozoic depositional system of the Caucasus. The fact that samples on the northern slope and near the western margin of the Greater Caucasus (ILN#13_700 and WC139/1; Figure 9a) have a close affinity to samples of the Eurasian interior (Figure 8a) suggests that detritus from the Eurasian interior was deposited to the north of the Greater Caucasus and also to the south of the westernmost portion of the range (Figure 4). In contrast, the detrital zircon age distribution of sample WG66c/2 (Figure 9a) includes the major age peaks of the Greater Caucasus siliciclastic sequence (Figure 8e), suggesting that at the longitude at which it was deposited, sediment was sourced primarily from the Greater Caucasus (Figure 5b). Sample WC99/3 (Figure 9a), deposited on the southern slope of the Greater Caucasus at an intermediate longitude between WC139/1 and WG66c/2 (Figure 4) shows a hybrid detrital zircon age signature suggesting mixing of the Eurasian interior and Greater Caucasus siliciclastic sequence sources. Together, these samples define a spatial mixing trend where the Eurasian interior is the dominant detrital zircon source affinity of Neogene sediment on the north side of the Greater Caucasus and in the far western portion of the basin to the south of the Greater Caucasus, whereas the Greater Caucasus siliciclastic sequence is the dominant source affinity of Neogene deposits on the southern margin of the central to western Greater Caucasus (Figures 4 and 5).

The spatial distribution of detrital zircon affinities to the Eurasian interior and Greater Caucasus siliciclastic sequence mirrors the distribution of quartzose and lithic-rich sandstones, respectively, in Oligocene to Pliocene deposits

on the north-eastern margin of the Black Sea (Vincent et al., 2013; Vincent, Hyden, & Braham, 2014). Quartzose sandstone is observed in Neogene sedimentary rocks to the north of the Greater Caucasus and in the far western portion of Neogene sedimentary rocks on the south side of the range (west of 40° E; Vincent et al., 2013, 2014). The distribution of quartzose sandstone corresponds spatially with detrital zircon age signatures of Eurasian affinity (Figure 4; samples ILN#13_700 and WC139/1 in Figure 9a). In contrast, lithic-rich sand containing mudstone and volcanic fragments is observed in Neogene sedimentary rocks from the western Greater Caucasus (east of 40° E; Vincent et al., 2013, 2014), in the same region where Oligocene to Miocene sandstones reveal a detrital zircon age signature similar to the Greater Caucasus siliciclastic sequence (Figure 4; samples WC99/3 and WG66c/2 in Figure 9a). The correspondence of quartz-rich sandstones with zircon ages of Eurasian affinity and of lithic-rich sandstones with zircon of Greater Caucasus siliciclastic affinity may reflect differing source area lithologies or the longer transport distance, and thus probably greater maturity, of sediment from the Eurasian interior.

6.2 | Western foreland basin section

Our western foreland basin section contains five samples spanning Oligocene to Quaternary age (Figures 9b, S2b) that were collected from a ~2.3 km thick sedimentary section exposed along the Chanistskali River near Jvari, Georgia (Figure 5b; Dzhanelidze & Kandelaki, 1957). The section consists of organic-rich shales, marls and turbiditic sandstones of Oligocene to Middle Miocene age (Maikopian through Badenian regional stages; ~35–10.5 Ma; Dzhanelidze & Kandelaki, 1957, Figure 10b) that pass upward into conglomerates, sandstones and mudstones of Late Miocene (Sarmatian regional stage; 10.5–8.2 Ma; Jones & Simmons, 1997) to Quaternary age (Dzhanelidze & Kandelaki, 1957, Figure 10b). Late Miocene and younger strata in the western Greater Caucasus are interpreted as having been deposited in a largely terrestrial environment (Vincent et al., 2014). The two oldest samples from the western section, WF-1 and WF-2, were collected from Oligocene to Middle Miocene sandstones (Figure 6a shows sample location of WF-2) and show dispersed Proterozoic to Triassic ages with wide peaks centred on 450 Ma and 300 Ma (Figure 9b) and ~25% of ages >900 Ma. WF-1 and WF-2 have a zircon age peak at 170 Ma, as well. The age peaks of these two samples correspond well with samples of the Greater Caucasus siliciclastic sequence (Figure 8e). The three youngest samples collected from the section, samples WF-3, WF-4, and WF-5, were collected from latest Pliocene to Quaternary terrestrial conglomerates (Figure 6b shows sample location of WF-3). Sample WF-3 is dominated by a 170 Ma peak, along with small, wide peaks

at ~300 Ma and ~450 Ma (Figure 9b). The dominance of the 170 Ma age peak in sample WF-3 suggests affinity to the western Greater Caucasus volcanoclastic sequence (samples CT130924-9A, WGC-3 in Figure 8f). Sample WF-3 also shows a concentration of zircon ages from 3 to 2.5 Ma, which likely originate from the eruption of the Chegem caldera in the northern Greater Caucasus at ~2.8 Ma (Lipman et al., 1993). Samples WF-4 and WF-5 have tightly clustered ~300 Ma and ~450 Ma age peaks, and have 7–8% zircon ages >900 Ma, significantly fewer than stratigraphically lower samples WF-1 and WF-2 (Figure 9b). The tight clustering of the ~300 Ma and ~450 Ma age peaks and smaller portion of ages >900 Ma in samples WF-4 and WF-5 differentiate these samples from WF-1 and WF-2 and suggest that WF-4 and WF-5 have an affinity to the Greater Caucasus basement, rather than the Greater Caucasus siliciclastic sequence.

The three sources most similar to the age spectra observed in the western section are the Greater Caucasus siliciclastic sequence (Figure 8e), Greater Caucasus volcanoclastic sequence (Figure 8f) and the Greater Caucasus basement (Figure 8b), all of which are located to the north of the section, so the observed provenance changes likely reflect changing exposure within the sediment source area. Therefore, we regard the provenance changes in the western section as recording the exposure of the volcanoclastic strata and the basement of the Greater Caucasus as a result of progressive deformation, unroofing and erosion of the range. The age of first exposure of the Greater Caucasus volcanoclastic strata is uncertain, but is bracketed by Middle Miocene sample WG66c/2 (Vincent et al., 2013), which is located near our sampled section and which shows no evidence of derivation from the volcanoclastic strata, and late Pliocene sample WF-3, which is dominated by ~170 Ma ages. Samples WF-4 and WF-5 record initial exposure of the Greater Caucasus basement in the sedimentary source area during latest Pliocene to Quaternary time. Combining the detrital zircon age data with stratigraphic observations (Figure 10b) reveals that the initial exposure of basement, and potentially the initial exposure of the Greater Caucasus volcanoclastic strata, followed the transition to terrestrial sedimentation within the western Caucasus.

An analysis of recycled palynomorphs from the same section that we sampled also constrains the unroofing history of the western Greater Caucasus (Vincent et al., 2014). Successively older palynomorphs are found stratigraphically higher in the section, which suggests the exhumation of progressively deeper strata over time in the source area (Vincent et al., 2014). In Early Oligocene time, the oldest palynomorphs observed are of Eocene age. Beginning in Late Oligocene time, palynomorph assemblages imply source ages as old as Early Cretaceous, with a significant portion of Eocene palynomorphs also present. In Early Miocene time, the prevalence of Eocene palynomorphs decreases and recycled palynomorphs transition to predominantly Cretaceous

age. A small number of palynomorphs in Early Miocene strata imply Middle Jurassic source ages (Vincent et al., 2014). Though no samples younger than Early Miocene were analysed (Vincent et al., 2014), the exhumation history implied by these samples is consistent with eventual exposure of basement in the sedimentary source area during Pliocene to Quaternary time.

6.3 | Central foreland basin section

Our central foreland basin section (Figures 9c, S2c) contains two samples of Middle and Late Miocene age, collected from a 5- to 7.5-km thick Oligocene to Quaternary succession 30 km north-east of Tbilisi, Georgia (Figure 5a; Edilashvili, 1957). In the sampled section, Oligocene to Miocene mudstones, marls and sandstone interlayers of the Maykopian to middle Sarmatian regional stages (~36–~9 Ma; Edilashvili, 1957, Figure 10c) pass upward into sandstones, variegated mudstones and coals of the Late Miocene upper Sarmatian regional stage (~9–8.2 Ma; Edilashvili, 1957, Figure 10c), which are overlain by Late Miocene sandstones and conglomerates of the Meotian to Pontian regional stages (8.2–5.3 Ma; Edilashvili, 1957, Figure 10c). Sample CF-1 was taken from a Middle Miocene (pre-Sarmatian) sandstone bed within a shale-rich sequence (Figure 6c). CF-1 contains zircon ages <90 Ma and age peaks centred on 300 Ma and 170 Ma (Figure 9c), a very similar age distribution to modern samples of the Lesser Caucasus (Figure 8b). Sample CF-1 also contains two ~15 Ma zircon grains, which provide a maximum depositional age. Upsection, Late Miocene (Meotian to Pontian) terrestrial conglomerate sample CF-2 (Figure 6d) has dispersed Proterozoic to Mesozoic zircon ages with wide peaks centred on 450–400, 300, and 170 Ma (Figure 9c), indicating affinity to samples of the Greater Caucasus siliciclastic sequence (Figure 8e).

The transition of sediment source from the Lesser Caucasus to the Greater Caucasus observed in the central foreland basin section is most simply explained by tectonic translation towards the Greater Caucasus via subduction/shortening. At the outcrop from which CF-1 was collected, folding within isolated strata between undeformed stratigraphic packages suggests that syn-sedimentary slumping occurred (Figure 6c). Given the Lesser Caucasus provenance of CF-1 (Figure 9c) and the shale-rich lithology and syn-sedimentary deformation of the outcrop from which it was collected, CF-1 was likely deposited on the Lesser Caucasus basin margin, in an environment similar to a continental slope. The Greater Caucasus affinity of sample CF-2 indicates that before the end of the Pontian regional stage (5.3 Ma; Jones & Simmons, 1997), the sedimentary source had switched from the Lesser Caucasus to the Greater Caucasus. The central section also contains a Pliocene hiatus of similar timing and duration to the western section (Figure 10).

6.4 | Eastern foreland basin section

Samples from the eastern section (Figures 9d, 10d and Figure S2d) span almost the entire Cenozoic, from latest Cretaceous or Palaeocene time until Pliocene time, and were collected from a 6- to 7.5-km thick composite section (Figure 5c; Khain & Shardanov, 1960). Within this section, a transition from marine sandstone, organic-rich shale and marl deposition to largely terrestrial, conglomeratic deposition occurred in latest Miocene time (Pontian regional stage) to earliest Pliocene time (Kimmerian regional stage; Khain & Shardanov, 1960). Most samples from this section (samples EF-2 through EF-6) were collected near Lahij and Shamakhi, Azerbaijan. Late Cretaceous to early Palaeocene sample EF-1 was collected from the north side of the Greater Caucasus, near the village of Afurgha, Azerbaijan, though it was deposited prior to shortening and topographic development in the Greater Caucasus (which began in late Eocene to Oligocene time; Adamia, Alania, Chabukiani, Kutelia, & Sadrade, 2011; Vincent et al., 2007), and is thus inferred to have been deposited in the same basin as samples EF-2 through EF-6. Samples EF-1 to EF-5 were collected from marine sandstone-shale sequences of Palaeogene through Late Miocene age (Figure 6e shows the shale-rich interval from which EF-4 was collected). EF-1 through EF-5 reveal a consistent detrital zircon age signature featuring dispersed Proterozoic to Triassic ages, typically with peaks centred on 400–450 Ma and 300 Ma (Figure 9d). Age peaks centred on 170 Ma are also sometimes present, and Oligocene to late Miocene samples in this section also show some ages from 60 to 30 Ma. Overall, samples EF-1 to EF-5 show a strong similarity to modern samples of the Greater Caucasus siliciclastic sequence (Figure 8e). The Cenozoic grains in samples EF-3, EF-4 and EF-5 are likely to have originated in Cenozoic volcanic centres of the Lesser Caucasus and neighbouring Talysh mountain ranges (Allen & Armstrong, 2008; van Der Boon et al., 2017; Verdel, Wernicke, Hassanzadeh, & Guest, 2011). These Cenozoic zircon grains could have been transported by turbidity currents and mixed with Greater Caucasus-derived sediment within the basin, or they could have been deposited in the basin as volcanic airfall and subsequently reworked. We tentatively favour the latter interpretation because samples EF-3, EF-4 and EF-5 lack the major Jurassic and Cretaceous age peaks that characterize modern and foreland basin samples derived from the Lesser Caucasus (samples LC-1 to LC-4, Figure 8c; CF-1, Figure 9c). Together, samples EF-1 to EF-5 indicate derivation from the Greater Caucasus siliciclastic sequence from Late Cretaceous or Palaeocene time until Late Miocene time.

Pliocene sample EF-6 (Figure 6f) was collected from a sandstone horizon of the thick, fluvio-lacustrine Productive

Series (e.g. Hinds et al., 2004). The detrital zircon U-Pb age distribution of EF-6 shows scattered Proterozoic to Cenozoic zircon ages with peaks centred on ~300 Ma, 160 Ma, 105 Ma, and 85 Ma, with many additional ages <85 Ma (Figure 9d). These age peaks indicate affinity to the Lesser Caucasus arc sequence (Figure 8c). However, EF-6 also contains Precambrian zircon ages and a wide ~450 Ma age peak, indicating affinity to the Greater Caucasus siliciclastic sequence (Figure 8e) in addition to the Lesser Caucasus arc sequence (Figure 8c). Heavy mineral provenance from Productive Series strata in the same region also suggest derivation from the Lesser Caucasus (Morton et al., 2003), and some palaeocurrents within the Productive Series are oriented towards the east (Vincent, Davies, Richards, & Aliyeva, 2010), similar to the modern Kura River (shown in Figure 5a).

The contrasting provenance and lithology between the Pliocene, fluvio-lacustrine Productive Series (sample EF-6) and pre-Pliocene underlying marine sandstone-mudstone sequences (samples EF-1 to EF-5) suggest a significant change in the drainage network. Detrital zircon ages in the pre-Pliocene organic-rich sandstone-shale intervals (samples EF-1 through EF-5) suggest derivation from the Greater Caucasus to the north. In contrast, the presence of Lesser Caucasus-derived material (sample EF-6; Morton et al., 2003) and eastward palaeocurrent directions (Vincent et al., 2010) in the Pliocene Productive Series suggest deposition in a longitudinal drainage that included both Greater and Lesser Caucasus sources within its catchment. The Productive Series was deposited over 2–3 Myrs beginning in the earliest Pliocene (5.3 Ma) and attains thicknesses of 4–5 km in the Kura-South Caspian region (Green, Abdullayev, Hossack, Riley, & Roberts, 2009; Vincent et al., 2010), whereas the entire Oligo-Miocene sequence attains a maximum thickness of 2.5 km (Green et al., 2009), indicating an increase in sedimentation rate coincided with this change in provenance. Deposition of the Productive Series, including sample EF-6, would have roughly coincided with non-deposition or erosion in the western and central foreland basin sections (Figure 10b–d), suggesting that some Productive Series sediment may have been eroded from the western foreland basin. The Pliocene deposition of Greater- and Lesser Caucasus-derived sediment in the eastern foreland basin and erosion in the western foreland basin may reflect an absence of accommodation between the Greater Caucasus and Lesser Caucasus at the longitude where the continents were in closest proximity to one another.

6.5 | Far eastern foreland basin section

The far eastern section consists of previously published samples from the Pliocene Productive Series sandstones on the Apsheron Peninsula in easternmost Azerbaijan (Figures 4,

9e, 10e, S2e; Allen et al., 2006). We note that this section covers a smaller range of geologic time than the western, central and eastern sections discussed above (Figure 10). These samples show a virtually constant detrital zircon age signature through time that features a majority of ages >900 Ma, with scattered Neoproterozoic to Mesozoic ages that coalesce around ~300 Ma and 400–450 Ma age peaks in some samples (Figure 9e). A subsequent detrital zircon study with greater sampling resolution of this section revealed similar age signatures (Abdullayev et al., 2018). The concentration of zircon ages >900 Ma in these samples indicates affinity to the age signatures of the Eurasian interior (Figure 8a), with the wide ~300 Ma and 400–450 Ma age peaks of some samples suggesting affinity to the Greater Caucasus siliciclastic strata (Figure 8e), as well.

7 | TECTONIC CONTEXT OF OBSERVED ZIRCON CRYSTALLIZATION AGES

7.1 | Cenozoic zircon ages

Cenozoic zircon ages are found primarily in samples derived from the Lesser Caucasus (Figure 8c), and they are also present in small quantities in several samples that otherwise appear to be derived from Greater Caucasus sources (samples WF-3, EF-3, EF-4, EF-5; Figure 9). The Lesser Caucasus was the site of a Mesozoic to Eocene arc, as well as subsequent volcanism that spanned the Oligocene to Quaternary (Adamia, Zakariadze, et al., 2011; Dilek, Imamverdiyev, & Altunkaynak, 2010; Nalivkin, 1976; Sahakyan et al., 2017). The western Greater Caucasus hosts Pliocene to Quaternary volcanic centres (Lipman et al., 1993), and also contains small, isolated intrusions of Neogene age (Nalivkin, 1976). Given the close age correspondence between late Cenozoic zircon ages in sample WF-3 (2.5–3 Ma; Figure 9b) and the eruption of Chegem caldera in the western Greater Caucasus (2.8 Ma; Lipman et al., 1993), Chegem is a likely source for the young detrital zircon ages of WF-3. No Cenozoic volcanic centres are known in the eastern Greater Caucasus, so we attribute Cenozoic zircon ages in eastern foreland basin samples EF-3, EF-4, and EF-5 (Figure 9d) to volcanic airfall from the Lesser Caucasus and neighboring Talysh.

7.2 | Permian to Mesozoic zircon ages

Cretaceous zircon ages are found in samples from the Lesser Caucasus (Figure 8c), the Greater Caucasus siliciclastic sequence (Figure 8e), and the Greater Caucasus volcanoclastic sequence (Figure 8f). In the Lesser Caucasus arc sequence (Figure 8c), Cretaceous zircon grains are common and likely

were crystallized during Mesozoic arc volcanism (Adamia, Zakariadze, et al., 2011; Rolland et al., 2011; Sosson et al., 2010). In the Greater Caucasus siliciclastic sequence (Figure 8e), Cretaceous zircon grains are likely derived by volcanic airfall from the Lesser Caucasus, which is the nearest known centre of Cretaceous volcanism (Rolland et al., 2011; Sosson et al., 2010). Cretaceous zircon ages dominate the eastern Greater Caucasus volcanoclastic sequence, which is Cretaceous in age (Kopp, 1985; Nalivkin, 1976), defining a single narrow detrital zircon age peak at 105 Ma (Figure 8f).

Jurassic zircon ages are observed in samples of the Lesser Caucasus arc sequence (Figure 8c), the Greater Caucasus siliciclastic sequence (Figure 8e) and the Greater Caucasus volcanoclastic sequence (Figure 8f). Jurassic intrusions have been recognized in all three sequences (Hess, Aretz, Gurbanov, Emmermann, & Lippolt, 1995; Nalivkin, 1976). The Jurassic marked the initiation of arc volcanism in the Lesser Caucasus and the initial rifting of the Greater Caucasus basin (Sosson et al., 2010; Vincent et al., 2016; Zonenshain & Le Pichon, 1986), so it is unsurprising that Jurassic zircon ages were generated in association with these settings and are common throughout the region. Because Jurassic zircon ages are ubiquitous in Jurassic and younger sedimentary sequences throughout the Caucasus, they are not useful for differentiating between potential sediment sources.

Permian to Triassic zircon ages are observed in significant quantity only in the Greater Caucasus siliciclastic sequence (Figure 8e) and foreland basin sediments inferred to be sourced from it. Such Permian to Triassic grains are likely derived from Permian and Triassic volcanic and volcanoclastic rocks that overlie the Greater Caucasus basement on the northern slope of the range (Belov, 1981; Nazarevich, Nazarevich, & Shvydko, 1986).

7.3 | Precambrian to Carboniferous zircon ages

Pre-Permian zircon ages in the Caucasus reflect the crystallization history of regional basement domains. A ~300–360 Ma age peak is ubiquitous in the Greater Caucasus basement (Figure 8b), Transcaucasus basement massifs (Figure 8c) and the Greater Caucasus siliciclastic sequence (Figure 8e), as well as younger sedimentary strata derived from these sources (Figure 9). The 300–360 Ma age peak reflects crystallization within or simultaneous with the Variscan orogeny, when a Gondwana-derived ribbon continent that may have included the Greater Caucasus and Transcaucasus basement terranes was accreted to the southern margin of Eurasia (Stampfli & Borel, 2002; Stampfli, Hochard, Verard, & Wilhelm, 2013), driving high temperature–low pressure metamorphism and magmatism in the Caucasus region (Belov, Somin, & Adamiya, 1978; Somin, 2011). The

Greater Caucasus basement and Greater Caucasus siliciclastic sequence also contain a ~450 Ma age peak, typically in subequal proportion to the ~300 Ma age peak (Figure 8b, e). In our samples from modern rivers that drain the Greater Caucasus basement, this ~450 Ma age peak is likely sourced from pre-Carboniferous metamorphic complexes that constitute part of the Greater Caucasus basement (Somin, 2011). Ages of ~450 Ma correspond to a period when the Greater Caucasus basement has been proposed to have undergone arc volcanism during transit from Gondwana to Laurussia as part of the superterrane Hunia (Stampfli, 2013; Stampfli et al., 2013). Alternatively, 450 Ma ages are observed in the Nubian shield, suggesting that ~450 Ma ages observed in the Greater Caucasus basement may have crystallized on the Gondwanan margin (Abdel-Rahman & Doig, 1987; Höhndorf, Meinhold, & Vail, 1994). The presence of 300–360 and 450 Ma age peaks in samples of the Greater Caucasus siliciclastic sequence (Figure 8e) indicates that the source region of this sequence may have undergone a history of metamorphism and magmatism similar to that of the Greater Caucasus basement. 600–900 Ma zircon ages are observed in minor proportions in many samples of Greater Caucasus basement (Figure 8b), Transcaucasus basement massifs (Figure 8c), and Greater Caucasus siliciclastic sequence (Figure 8e). These zircon ages suggest an affinity to the Pan-African orogeny, which occurred on Gondwana (e.g. Avigad, Kolodner, McWilliams, Persing, & Weissbrod, 2003; Johnson & Woldehaimanot, 2003; Horton et al., 2008; Stern & Johnson, 2010; Johnson, 2014; Vasey et al., 2020). Pre-900 Ma zircon ages are present in our study mostly in the modern detritus of the Eurasian interior as well as sedimentary strata likely derived in part from the Eurasian interior. Zircon grains of this age are associated with the East European Craton (Allen et al., 2006; Bogdanova et al., 2008).

8 | IMPLICATIONS FOR LATE CENOZOIC EVOLUTION OF THE CAUCASUS AND STRATIGRAPHIC RECORDS OF COLLISION

8.1 | Late Cenozoic provenance and lithological changes of Caucasus foreland basin sedimentation

Dramatic changes in sediment composition and provenance occurred in the Caucasus during late Cenozoic time (Figure 11). Pre-Middle Miocene strata consist of organic-rich, turbiditic to deltaic sandstone-shale sequences inferred to have been deposited in a marine environment (Figure 10; Vincent et al., 2007; Hudson et al., 2008). Detrital zircon U-Pb age distributions from pre-Middle Miocene samples imply sourcing from either the Greater Caucasus or the Lesser Caucasus, with no

observed mixing of source signatures (Figure 9). Detrital zircon provenance of the central section reveals that Greater Caucasus detritus was deposited on the Lesser Caucasus basin margin slope sometime between 15 Ma and 5.3 Ma (Figure 9c; event 1 in Figure 11a), suggesting the subduction/underthrusting of the Lesser Caucasus basin margin during that time interval. The western and central sampled sections, which lie broadly within the western Greater Caucasus where collision has been hypothesized to have begun in latest Miocene to Pliocene time (Avdeev & Niemi, 2011; Cowgill et al., 2016; Philip et al., 1989), indicate a transition to terrestrial and largely conglomeratic sedimentation during Late Miocene time, around 10.5 to 8.5 Ma (Figure 10b, c; event 2 in Figure 11a). At the Miocene to Pliocene transition (~5.3 Ma), a hiatus began in the western and central sections (10b, c; event 3 in Figure 11a), coeval with deposition of a thick package of Lesser- and Greater Caucasus-derived sediment in a longitudinal drainage network in the eastern foreland basin (Figures 9d, 10d; event 4 in Figure 11a). Finally, in latest Pliocene or Quaternary time (<2.8 Ma), the first sediment derived from Greater Caucasus basement was deposited in the western foreland basin (Figure 9b; event 5 in Figure 11a).

8.2 | Drivers of observed lithology and provenance changes

Potential drivers of late Cenozoic changes in depositional environment and provenance across the Caucasus foreland basin include collision between the Greater and Lesser Caucasus blocks, regional base level changes that occurred throughout the Paratethyan system at this time (Forte & Cowgill, 2013; Krijgsman et al., 1999; Krijgsman, Stoica, Vasiliev, & Popov, 2010; Vasiliev, Reichart, & Krijgsman, 2013; Zubakov, 2001), climatic changes or autogenic processes. To determine the effects of these potential drivers, we compare the timing of observed sedimentary changes with the timing of Caucasus collision and the timing of late Cenozoic regional base level changes.

8.2.1 | Transition from subduction to collision

The Greater Caucasus underwent several structural and kinematic changes during late Cenozoic time, many of which are temporally associated with the changes in sedimentary lithology and provenance outlined above. Following the initiation of deformation in the Greater Caucasus at 35 Ma (Adamia, Zakariadze, et al., 2011; Vincent et al., 2007), the upper plate was exhumed slowly (~0.1 mm/yr) during Oligocene to Miocene time as inferred from thermochronometry data (Avdeev & Niemi, 2011; Vincent et al., 2011). This period

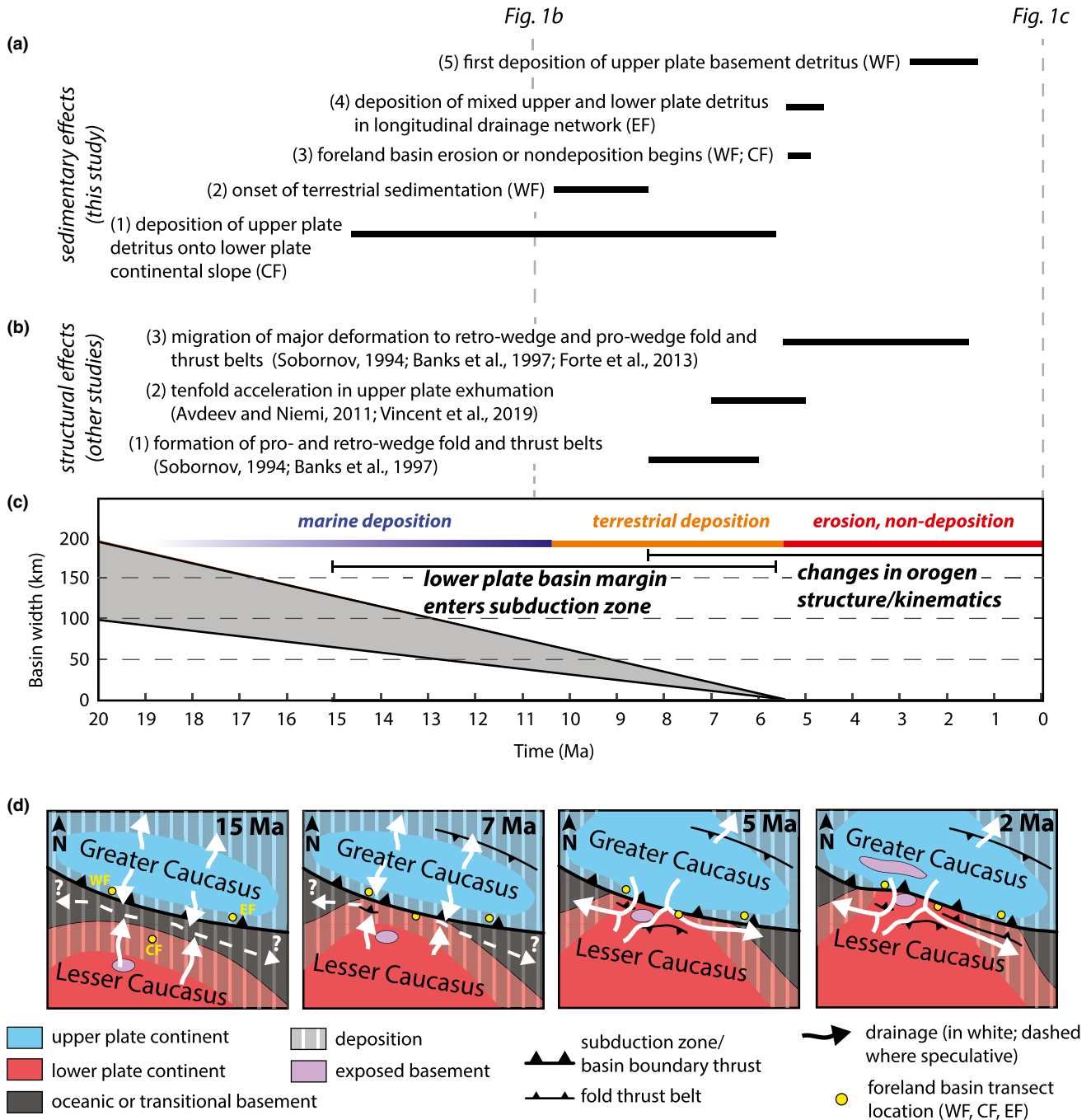


FIGURE 11 A timeline of sedimentary and structural effects of collision is developed from observations in the Caucasus. (a) Transitions in foreland basin sediment provenance and composition are inferred from our detrital zircon U-Pb age data and published stratigraphy. Each event is numbered for reference in the text and labelled parenthetically with the foreland basin section from which it was inferred (WF—western, CF—central, EF—eastern). (b) Structural changes in the orogen are reported from other studies, numbered and labelled with references. Vertical dashed lines indicate the ages associated with the timesteps of collision shown in Figure 1. (c) Basin width, foreland sedimentation style, and phase of collision are plotted against time. Basin width is inferred using timing estimates of Greater and Lesser Caucasus convergence and width estimates of the intervening basin (see Section 8.3 for further discussion). The grey shaded region indicates an uncertainty envelope based on variability in basin width estimates. (d) Schematic map view reconstruction of the late Cenozoic tectono-sedimentary evolution of the Caucasus

of slow exhumation coincided with deposition of organic-rich, turbiditic and deltaic sequences between the Greater and Lesser Caucasus, likely in a marine setting, until Middle to Late Miocene time (Figures 10 and 11; Vincent et al.,

2007; Hudson et al., 2008). Prior to Middle Miocene time, detrital zircon ages in the western and eastern foreland basin sections indicate derivation exclusively from the Greater Caucasus, implying transport from the north. In contrast,

detrital zircon grains of the central foreland basin section are derived from the Lesser Caucasus, implying transport from the south. Given the compressional deformation occurring in the Greater Caucasus during this time (Adamia, Zakariadze, et al., 2011; Vincent et al., 2007), the slow Greater Caucasus exhumation rates and presence of a marine basin between the Greater and Lesser Caucasus until at least Middle Miocene time are consistent with Greater Caucasus–Lesser Caucasus convergence being accommodated by subduction of the basin floor during Oligocene to Middle Miocene time.

Several structural and sedimentary transitions took place in the Caucasus during Middle to Late Miocene time. Between 15 and 5.3 Ma, deposition of Greater Caucasus detritus onto the Lesser Caucasus basin margin is recorded in the central foreland basin section (Figure 10), which in other orogens has been inferred to reflect entrance of the lower plate continental margin into the subduction zone (Figure 11a; DeCelles et al., 2014; Garzanti et al., 1987; Hu et al., 2015; Najman et al., 2010). During Late Miocene time, deformation began within the Dagestan retro-wedge fold and thrust belt (Sobornov, 1994) and the Tsaishi anticline, a pro-wedge fold-thrust structure to the south of the western Greater Caucasus (Banks et al., 1997). Deformation within these fold and thrust belts reflects migration of strain away from a single, dominant structure that previously accommodated convergence. In models of incipient collision zones, the development of fold and thrust belts corresponds with locking of the subduction zone thrust due to the increasing thickness and buoyancy of lower plate material being subducted (Beaumont et al., 1996; Regard et al., 2003; Toussaint et al., 2004). Sedimentary strata deposited between the Greater and Lesser Caucasus began to transition during Middle to Late Miocene time from turbiditic sandstones and organic-rich shales to conglomeratic red beds inferred to reflect terrestrial depositional environments (Figures 10 and 11). The timing of terrestrial deposition suggests it was caused by decreasing accommodation space between the Greater and Lesser Caucasus as well as structural uplift above new thrust faults in some locations. The combination of deposition of Greater Caucasus detritus onto the Lesser Caucasus basin margin, initiation of fold and thrust belt deformation, and transition to terrestrial depositional environments is consistent with incipient collision between the Lesser Caucasus arc terrane and the Greater Caucasus orogen during Late Miocene time, following subduction/underthrusting of the intervening basin crust.

During latest Miocene to Pliocene time, structural changes within the orogen intensified, coinciding with changes in foreland basin sediment routing. Thermochronometry data suggest that exhumation of the Greater Caucasus increased by a factor of 10, to ~ 1 mm/yr, at 7–5 Ma (Avdeev & Niemi, 2011; Vincent et al., 2020), likely reflecting accretion of lower plate material as predicted by some models in

the early stages of collision (Toussaint et al., 2004, Figure 11b). Pliocene to Quaternary time is reported as the period of major activity on retro- and pro-wedge fold and thrust structures that first developed in Late Miocene time (Banks et al., 1997; Sobornov, 1994, Figure 11b). These Pliocene structural changes coincide with erosion or non-deposition in the western to central foreland basin (Figures 10 and 11a,d). The transition to erosion or non-deposition in the western to central foreland basin coincided with longitudinal transport and mixing of Greater- and Lesser Caucasus-derived sediments and their deposition in the Kura and South Caspian basins (Figures 10 and 11). The coeval transition to erosive conditions in the western to central foreland and longitudinal transport of Greater- and Lesser Caucasus-derived sediments to the east is consistent with increasing proximity and deformation between the Lesser Caucasus arc terrane and Greater Caucasus orogen.

The structural and sedimentary conditions of the Pliocene largely continued to the Quaternary. The oldest observed foreland basin sample inferred to be derived from the Greater Caucasus basement was deposited after 2.8 Ma (Figures 10 and 11a), suggesting that initial exposure of basement in the sedimentary source area followed the increase in exhumation rate that occurred in latest Miocene to Pliocene time (Avdeev & Niemi, 2011; Vincent et al., 2020). The pro-wedge fold and thrust belt of the Kura basin underwent initial deformation at ~ 2 –1.5 Ma (Figure 11b,d; Forte et al., 2013, 2014). At present, deformation across most of the orogen is accommodated by fold and thrust belts off the subduction zone (Forte et al., 2013; Sokhadze et al., 2018), contiguous elevated topography stretches between the western Greater Caucasus and the Lesser Caucasus (Figure 2d), and longitudinal drainages are located between the two ranges (Figure 2a).

8.2.2 | Paratethys base level changes

In addition to the late Cenozoic tectonic evolution of the Caucasus, Miocene to Pliocene sedimentation may also have been affected by base level changes in the Paratethyan basin system of which the Caucasus foreland basin was part (e.g. Forte & Cowgill, 2013; Popov et al., 2006; van Baak et al., 2015, 2017). Base level falls of up to several hundred metres may have occurred in the Black Sea and the Caspian Sea during Late Miocene to Pliocene time, potentially as a result of disconnection between the Atlantic Ocean and Mediterranean Sea during the Messinian Salinity Crisis (Forte & Cowgill, 2013; Krijgsman et al., 1999, 2010; van Baak et al., 2017; Vasiliev et al., 2013; Zubakov, 2001). This base level fall would have also reduced base level in the basin between the Greater and Lesser Caucasus, which is likely to have served as a connection between the Black and Caspian seas prior to its closure during Late Miocene to Pliocene time (Popov

et al., 2006; Zonenshain & Le Pichon, 1986). Low Black Sea base levels lasted from 5.6 Ma until 5.4 Ma (van Baak et al., 2015), whereas low base levels in the Caspian appear to have persisted from latest Miocene time until 4–2.7 Ma (Forte & Cowgill, 2013; van Baak et al., 2019). Connectivity between the Black and Caspian Seas is inferred to have been severed in latest Miocene to earliest Pliocene time (Forte & Cowgill, 2013, and references therein), which our results show may be a result of collision between the Greater and Lesser Caucasus.

The short duration of low Black Sea base levels indicates that regional Paratethyan base level changes cannot by themselves account for the basin shallowing, terrestrial sedimentation and erosion/non-deposition observed in Caucasus foreland basin sections from Late Miocene time to the present. Changes in lithology and provenance observed in the Cenozoic Caucasus foreland basin correspond temporally with structural changes in the orogen that suggest basin closure and the initiation of Greater Caucasus–Lesser Caucasus collision (Figure 11). Many of the predicted sedimentary responses to collision discussed in Section 2 are observed, including coarsening and shallowing of the basin, mixing of upper and lower plate sediment in a longitudinal drainage, and sourcing of detritus from deeper crustal levels (Figure 1). Thus, we conclude that first order sedimentation patterns in the late Cenozoic Caucasus foreland basin were driven by Greater Caucasus–Lesser Caucasus collision. Changing regional base levels, along with climate and autogenic processes, are inferred to have played a subordinate role.

8.3 | Correlating basin width with changes in sedimentary lithology and provenance

Based on the observed correlation between structural and sedimentary changes likely to be driven by collision in the Caucasus, we infer that convergence and collision of the Greater and Lesser Caucasus is the primary driver influencing foreland basin sediment composition and provenance. Thus, the width of the basin between two converging continents may influence facies and provenance in pre-collisional to collisional basins, and stratigraphic records may be able to be used to infer the width of these closing basins at different points in time (e.g. Malkowski et al., 2017). We use a simple calculation to estimate the width of the closing basin at the time these changes occurred (Figure 11c). Estimates of pre-convergence basin width between the Lesser and Greater Caucasus range from 200–280 km from kinematic reconstructions using palaeomagnetic data (van der Boon et al., 2018) to 350–400 km by analogy to the Black Sea basins and South Caspian basin (Cowgill et al., 2016). The basin between the Greater and Lesser Caucasus is thought to have closed from 35 Ma (Adamia, Alania, et al., 2011) until 5.3 Ma, when the basin became dominantly erosive and no longer

accommodated sediment (Figure 10), and for simplicity we assume a constant convergence rate between 35 and 5.3 Ma. Assuming pre-convergence widths from 200 to 400 km and a constant convergence rate from 35 Ma until 5.3 Ma yields convergence rates of 7–13 mm/yr. Such rates are comparable to modern convergence rates in the eastern Greater Caucasus where subduction is inferred to be ongoing (Kadirov et al., 2012, 2015; Reilinger et al., 2006). Using this basin width reconstruction, we find that when upper plate detritus was deposited on the lower plate basin margin in the central section (15–5.3 Ma), the basin was <130 km wide (Figure 11c). When the basin transitioned to terrestrial sedimentation (10–8 Ma), its width was between 15 and 65 km (Figure 11c). When the basin became largely erosive (5.3 Ma), by definition the basin width was reduced to zero (Figure 11c). This reconstruction serves as a starting point for understanding the relationship between basin width, sedimentary lithology and provenance, and the initiation of collision.

8.4 | Comparison with other foreland basin systems

The evolution of the Caucasus foreland basin system, in addition to largely conforming to the hypothesis outlined in Section 2, shares several commonalities with the evolution of other foreland basin systems in collisional and non-collisional settings. The deposition of upper plate-derived detritus onto the lower plate is widely recognized in the India–Asia collision zone (DeCelles et al., 2014; Garzanti et al., 1987; Hu et al., 2015; Najman et al., 2010) and along the Arabia–Eurasia plate boundary (Koshnaw et al., 2019). Where such deposition can be inferred to have occurred on the lower plate continental margin, the age of deposition can be taken as an estimate of initial continental subduction (DeCelles et al., 2014). These studies mirror observations in our central section of upper plate detritus deposited stratigraphically above lower plate detritus inferred to be deposited in a continental slope-type setting (Figures 10 and 11).

Underfilled foreland basin systems featuring longitudinal drainages close to the thrust front, similar to that observed in the modern Caucasus foreland (Figures 2, 10 and 11), are expected to exist in orogens undergoing active thrusting and accretion (Burbank, 1992; Raines, Hubbard, Kukulski, Leier, & Gehrels, 2013). Given the increase in exhumation rate and activity on fold and thrust belts in the Greater Caucasus since the Pliocene (Avdeev & Niemi, 2011; Banks et al., 1997; Forte et al., 2013; Sobornov, 1994), we infer that significant accretion has occurred recently or is ongoing, increasing the mass of the orogen and driving foreland subsidence, resulting in the present drainage network. The drainage network of the Caucasus is also likely to be influenced by high topography on the lower plate driven by shortening in the Lesser

Caucasus (Banks et al., 1997) and thermal and dynamic uplift of the East Anatolian Plateau to the south (Göğüş & Pysklywec, 2008; Keskin, Pearce & Mitchell, 1998; Şengör, Ozeren, Genc, & Zor, 2003).

9 | CAUCASUS COLLISION EVOLUTION AND COMPARISON TO OTHER OROGENS AND MODELS

Because natural examples of the transition from subduction to collision are rare, analogue and numerical modelling have been used extensively to investigate the effects of collision (e.g. Beaumont et al., 1996; Chemenda, Mattauer, & Bokun, 1996; Faccenda, Minelli, & Gerya, 2009; Regard et al., 2003; Toussaint et al., 2004; Toussaint, Burov, & Jolivet, 2004). The late Cenozoic structural evolution of the Caucasus orogen and the stratigraphic record of associated basins suggests that collision between the Greater Caucasus orogen and the Lesser Caucasus arc terrane, following the closure of an intervening marine basin, occurred during Late Miocene time. The record of collision in the Caucasus may thus advance our understanding of collision by serving as a test case for the process.

9.1 | Model predictions

Analogue and numerical models of the transition from subduction to collision reveal many different possible evolutionary pathways of collisional plate boundaries that unfold over millions to tens of millions of years (Faccenda et al., 2009; Regard et al., 2003; Toussaint et al., 2004). In particular, the rate at which an orogen transitions from accommodating convergence via subduction to accommodating convergence by crustal shortening has been shown by models to depend on convergence rate, thermal structure, and composition (Regard et al., 2003; Toussaint et al., 2004). Stable subduction of hundreds of kilometres of continental lithosphere is associated with convergence rates of >25 mm/yr and cold subducting lithosphere (Moho temperature <550°C; Regard et al., 2003; Toussaint et al., 2004). In contrast, slower convergence rates and hotter lithosphere is associated with convergence accommodated via lithospheric shortening following initial subduction of the lower plate continental margin (Toussaint et al., 2004).

9.2 | Comparison with the Caucasus and other natural systems

The Caucasus and other collisional orogens may provide insight into whether the hypothesized relationships between

convergence rate, thermal structure, and lithospheric composition and continental subduction hold for natural systems. Collisional systems proposed to have undergone significant continental subduction during the initiation of collision include the Arabia–Eurasia collision (150–480 km; Ballato et al., 2011; Pirouz, Avouac, Hassanzadeh, Kirschvink, & Bahroudi, 2017) and the India–Asia collision (>500 km; Johnson, 2002, and references therein). These collision zones both have cratonic lower plates (Förster, Förster, Oberhansli, & Stromeyer, 2010; Sengupta, Corfu, McNutt, & Paul, 1996) and were characterized by convergence rates of 30 mm/yr (Arabia–Eurasia; McQuarrie, Stock, Verdel, & Wernicke, 2003) and 200 mm/yr (India–Asia; Patriat & Achache, 1984) during the initiation of collision.

The amount of continental subduction in the Caucasus collisional system has not been previously estimated. Given the constraints on pre-convergence width of the basin between the Greater and Lesser Caucasus (<400 km; Cowgill et al., 2016; van der Boon et al., 2018) and the timing of initial subduction of the Lesser Caucasus basin margin slope (15–5.3 Ma), and assuming a constant convergence rate from initiation of basin closure (35 Ma; Adamia, Zakariadze, et al., 2011; Vincent et al., 2007) until final closure around 5.3 Ma, the amount of Lesser Caucasus continental crust subducted beneath Eurasia following subduction of the Lesser Caucasus basin margin is <130 km. The Lesser Caucasus was affected by Mesozoic to Palaeogene arc volcanism (Adamia, Zakariadze, et al., 2011; Rolland et al., 2011; Sosson et al., 2010) and is located on the northern margin of East Anatolia, a region inferred to have undergone lithospheric removal and/or detachment of the subducted Neotethys slab in Middle to Late Miocene time (Göğüş & Pysklywec, 2008; Keskin et al., 1998; Şengör et al., 2003). Therefore, continental lithosphere of the Lesser Caucasus is likely to be hotter and weaker than the cratonic lithosphere of Arabia and India. In addition, convergence rates during Caucasus collision are likely to have been significantly lower (7–13 mm/yr, assuming a constant convergence rate from Oligocene to latest Miocene time; Figure 11) than the convergence rates inferred for the Arabia–Eurasia and India–Asia collision zones (McQuarrie et al., 2003; Patriat & Achache, 1984). Thus, the relatively small amount of continental subduction inferred for the Caucasus compared to the Arabia–Eurasia and India–Asia collisional systems is consistent with model predictions for a system with slower convergence and a weaker, hotter lower plate continental lithosphere. The thickness and composition of basement initially located between the Greater and Lesser Caucasus, which may have been several kilometres thicker and/or less dense than typical oceanic crust (Cowgill et al., 2016; Mangino & Priestley, 1998), may also have reduced the amount of continental subduction compared to a system with typical oceanic lithosphere due to reduced slab pull.

10 | IMPLICATIONS OF CAUCASUS DETRITAL ZIRCON U-Pb AGE DATA FOR TERRANE BOUNDARIES AND TETHYAN TECTONICS

At the longitude of the Caucasus, the number and location of tectonic sutures along the southern Eurasian margin remain uncertain. Such sutures may have guided subsequent deformation, as has been suggested in other tectonic settings (Fitzgerald et al., 2014; Jones & Tanner, 1995; Rusmore, Gehrels, & Woodsworth, 2001). Scythia is thought to have undergone a crystallization history distinct from that of the East European Craton (Saintot, Stephenson, et al., 2006), potentially due to a suture between Scythia and the craton. At the northern margin of the Greater Caucasus basement, several authors have identified an ophiolite emplaced during Carboniferous time (Adamia et al., 1981; Somin, 2011), suggesting a suture between the Greater Caucasus and Scythia. However, Natal'in and Şengör (2005) argue that the Greater Caucasus basement is part of Scythia that was displaced by Triassic strike-slip displacement, meaning that the present location of the ophiolite between the Greater Caucasus basement and Scythia may not reflect a true suture between the two domains. Several reconstructions place a suture between the Greater Caucasus and Transcaucasus basement domains (Şengör, 1984; Stampfli, 2013; van Hinsbergen et al., 2020), although other authors have suggested a shared history between the Greater Caucasus and the Dzirula Massif, the northernmost exposed Transcaucasus basement, based on petrologic and age similarities (e.g. Mayringer et al., 2011). South of the Transcaucasus, terrane boundary locations are less ambiguous because of the presence of ophiolites along the Sevan–Akera suture zone (e.g. Galoyan et al., 2009; Khain, 1975), the Bitlis–Zagros suture zone (e.g. Şengör & Yılmaz, 1981), and between South Armenia and the easternmost Taurides (e.g. Topuz, Candan, Zack, & Yılmaz, 2017; van Hinsbergen et al., 2020).

Our detrital zircon age data constrain the timing and significance of magmatic and metamorphic episodes affecting basement domains of the East European Craton, Scythia, the Greater Caucasus and the Transcaucasus, which add evidence for or against proposed sutures between these domains (Figure 12). Our modern samples directly characterize the crystallization histories of the Greater Caucasus basement (Figure 8b) and Transcaucasus basement (Figure 8c), and published samples reflect the crystallization history of the Eurasian interior (Allen et al., 2006; Wang et al., 2011, Figures 8a and 12). Sedimentary architecture (Sholpo, 1978) and field observations (Vincent et al., 2013) indicate that the Greater Caucasus siliciclastic sequence is derived from the north, suggesting that our samples from this sequence (Figure 8e) constrain the crystallization history of the Eurasian interior and/or Scythia. Unlike the Eurasian interior, detrital zircon age signatures from the Greater

Caucasus siliciclastic sequence contain a majority of ages <900 Ma, typically with peaks at 300 Ma and 450 Ma (Figure 8e). Because zircon grains of age <900 Ma are comparatively rare in samples of the Eurasian interior and do not cluster in clear age peaks at 300 Ma and 450 Ma (Figure 8a), it is likely that the <900 Ma detrital zircon grains of the Greater Caucasus siliciclastic sequence are derived from Scythia (Figure 12). The scattered >900 Ma ages present in Greater Caucasus siliciclastic sequence samples (Figure 8e) may be derived from the Eurasian interior. Because the crystallization ages indicated by these detrital zircon grains constrain the tectonic histories of the East European Craton (Allen et al., 2006; Wang et al., 2011), Scythia, the Greater Caucasus basement, and the Transcaucasus basement, they are likely to yield new insight into the locations of sutures on the southern margin of Eurasia and their role in guiding tectonic deformation on this complex plate margin.

10.1 | Detrital zircon U-Pb age constraints on whether Scythia, Greater Caucasus basement and Transcaucasus basement domains were formed on the Eurasian margin or were accreted

Central to locating terrane boundaries on the southern margin of Eurasia is determining whether Scythia, Greater Caucasus and Transcaucasus basement domains formed in situ on the Eurasian margin or whether they originated on Gondwana or as intra-oceanic island arcs. The East European Craton is associated with zircon ages >900 Ma (Allen et al., 2006; Wang et al., 2011). Past work has identified zircon of age 600–900 Ma as diagnostic of crystallization during the Pan-African orogeny, which occurred on Gondwana (Avigad et al., 2003; Horton et al., 2008; Johnson, 2014; Johnson & Woldehaimanot, 2003; Stern & Johnson, 2010). Zircon grains of this age are virtually absent from samples containing detritus from the East European Craton (Figure 8a). Our detrital zircon U-Pb ages from the Greater Caucasus siliciclastic sequence (which we infer to be derived from Scythia), Greater Caucasus basement, and the Transcaucasus basement indicate that 600–900 Ma ages are present in all three domains, suggesting that they all originated on Gondwana (Figure 8b,c,e). Whereas previously available data from Scythian basement were unable to differentiate whether Scythia was exotic to Eurasia (e.g. Saintot, Stephenson, et al., 2006), our data support the hypothesis that a suture divides Scythia from Eurasia (Figure 12). Our findings are consistent with the view that the Transcaucasus and Greater Caucasus basement domains are exotic to Eurasia (e.g. Ruban, 2007, 2013; Ruban, Zeffass, & Yang, 2007; Stampfli, 2013; Vasey et al., 2020). The age of accretion of Scythia, the Greater Caucasus, and Transcaucasus basement domains to Eurasia is bounded by the age of the Pan-African orogeny to be <600 Ma.

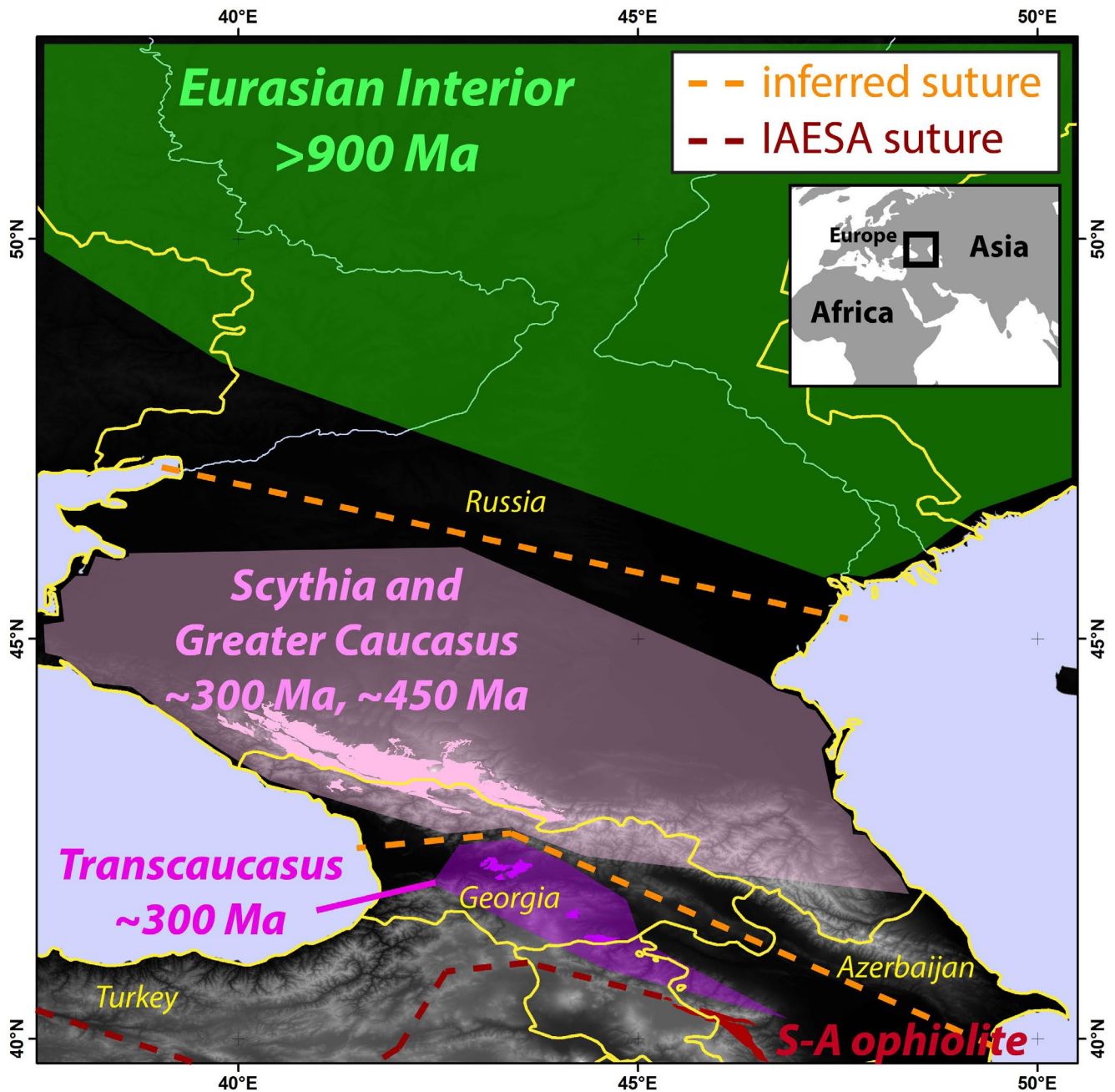


FIGURE 12 Crystallization ages inferred for basement domains from detrital zircon age data, and inferred suture locations between basement domains of shared crystallization history. Outcrops of crystalline basement in the Caucasus region are shown in opaque colour and areas of inferred basement composition are partially transparent. IAESA stands for Izmir-Ankara-Erzincan-Sevan-Akera suture, shown in dark red dashed line. S-A ophiolite stands for Sevan-Akera ophiolite, part of the IAESA suture, exposure of which is shown in dark red. See Section 10 for further discussion

10.2 | Detrital zircon age constraints on the similarities and differences between Greater Caucasus basement and Scythia

A suture between the Greater Caucasus basement and Scythia is suggested by ophiolites and eclogite-bearing blueschists in the northern Greater Caucasus that divide the two domains and that were emplaced in the Carboniferous (e.g. Adamia et al., 1981; Perchuk & Philippot, 1997; Philippot,

Blichert-Toft, Perchuk, Costa, & Gerasimov, 2001; Somin, 2011), although the Greater Caucasus and Scythia have also been proposed to constitute a single terrane disrupted and duplexed by Triassic strike-slip faulting (Natal'in & Şengör, 2005). If the Greater Caucasus basement and Scythia constitute a single terrane, the two domains would be expected to share a common crystallization and metamorphic history. If the Greater Caucasus basement is a separate terrane from Scythia, it is unlikely (though possible) that the Greater

Caucasus basement would share the crystallization history of Scythia. Detrital zircon ages from the Greater Caucasus basement cluster around age peaks at 300 Ma and 450 Ma (Figure 8b). Detrital zircon ages from the Greater Caucasus siliciclastic sequence, which we infer to be derived largely from Scythia, also cluster around age peaks at 300 Ma and 450 Ma (Figure 8e). The major difference between the age signatures of the Greater Caucasus basement and Greater Caucasus siliciclastic sequence is that the 300 Ma and 450 Ma age peaks are wider in the siliciclastic sequence samples (Figure 8e) than in the basement samples (Figure 8b). Assuming that the Greater Caucasus siliciclastic sequence was derived from a large region or regions of Scythia, this difference may reflect somewhat diachronous crystallization across Scythia, of which only a small portion is exposed in the Greater Caucasus basement. Pb loss or other complexities in preserved zircon U-Pb dates could exacerbate the difference in age peak width between the Greater Caucasus basement and Greater Caucasus siliciclastic sequence, but the lack of a systematic difference in discordance between the two sources (Figure S3) suggests that such complexities are not likely to be responsible for the entire observed difference in age peak width. Overall, our detrital zircon ages suggest that the Greater Caucasus basement has a similar crystallization history to Scythia, lending support to the hypothesis that the Greater Caucasus basement is part of Scythia, and suggesting that there is not a major terrane boundary between the Greater Caucasus basement and Scythia (Figure 12; Natal'in & Şengör, 2005). The presence of ophiolites in the northern Greater Caucasus may be attributable to strike slip duplexing of a single terrane (Natal'in & Şengör, 2005).

10.3 | Detrital zircon age constraints on the similarities and differences between Greater Caucasus basement and Transcaucasus basement

While several authors have proposed the existence of a suture between the Greater Caucasus and Transcaucasus basement (Adamia, Zakariadze, et al., 2011; Şengör, 1984; Stampfli, 2013; van Hinsbergen et al., 2020), others have noted age and compositional similarity between the Transcaucasus and Greater Caucasus (Mayringer et al., 2011; Zakariadze et al., 2007) and suggested a shared tectonic history between the two domains. The presence or absence of a suture here is important because the Greater Caucasus basin opened between the Greater Caucasus basement and Transcaucasus basement (Vincent et al., 2016; Zonenshain & Le Pichon, 1986). Thus, the opening of the Greater Caucasus basin may have been guided by a pre-existing structure between the Greater Caucasus and Transcaucasus. Our detrital zircon ages show that while the Greater Caucasus basement

contains subequal age peaks at 300 Ma and 450 Ma (Figure 8b), the Transcaucasus basement contains a 300 Ma age peak but does not contain a 450 Ma age peak (Figures 8c and 12). Our samples of the Greater Caucasus siliciclastic sequence (representing Scythia) indicate that 300 Ma and 450 Ma age peaks are subequal in size across much of Scythia (Figure 8e), in addition to within the Greater Caucasus basement (Figures 8b and 12). The fact that the Transcaucasus basement lacks such a pervasive and significant age peak compared to the Greater Caucasus and Scythia lends support to the hypothesis that a suture separates the Greater Caucasus and Transcaucasus (Figure 12; Adamia, Zakariadze, et al., 2011; Şengör, 1984; Stampfli, 2013; van Hinsbergen et al., 2020).

10.4 | Suture locations

The basement domain ages inferred from our detrital zircon data are consistent with the presence of two sutures between the Eurasian interior and the Transcaucasus, one between Eurasia and Scythia/Greater Caucasus and one between Scythia/Greater Caucasus and the Transcaucasus (Figure 12). These sutures were generated by the successive transit of terranes from Gondwana to the Eurasian margin (e.g. Şengör, 1984; Stampfli et al., 2013) and thus the sutures decrease in age from north to south (Yılmaz, Adamia, & Yılmaz, 2014). The ophiolites located to the south of the Transcaucasus, including the Sevan–Akera ophiolites (Figure 12) reflect sutures associated with Neotethys and are thought to have closed in Late Cretaceous time or later (Rolland et al., 2012; Sosson et al., 2010), indicating that the sutures we infer to the north of the Transcaucasus must predate Neotethys.

Up to three ocean basins have been proposed to exist between Gondwana/Africa and the Eurasian margin prior to Neotethys, termed the Qaidam, Rheic and Palaeotethys oceans (e.g. Şengör, 1984; Stampfli et al., 2013), and our inferred suture locations (Figure 12) are broadly consistent with multiple hypothesized locations of these sutures. Several authors infer that at the longitude of the Caucasus, the Palaeotethys suture coincides spatially with the Neotethys suture along the Sevan–Akera suture zone (Figure 12; e.g. Adamia, Zakariadze, et al., 2011; Stampfli, 2013). If this is the case, then the two sutures we infer between Eurasia and the Transcaucasus would represent the Qaidam and Rheic ocean sutures (Stampfli, 2013). However, other authors prefer to place the Palaeotethys suture between the Greater Caucasus and the Transcaucasus due to the lack of any pre-Triassic rocks, which would be expected for Palaeotethys, within the Sevan–Akera suture zone (e.g. Natal'in & Şengör, 2005; Şengör, 1984; van Hinsbergen et al., 2020). In this case, the inferred suture between Scythia and the Eurasian interior may correspond with the Qaidam

Ocean and the Rheic ocean suture may correspond spatially with either the Qaidam or Palaeotethys sutures. The opening and subsequent closure of the Greater Caucasus basin following the formation of these sutures is likely to have obscured evidence of any of these sutures located between the Greater Caucasus and Transcaucasus (Cowgill et al., 2016; van der Boon et al., 2018; van Hinsbergen et al., 2020).

11 | CONCLUSIONS

We present new detrital zircon U-Pb age data from the Caucasus that reveal temporally correlated changes in orogen structure and sediment provenance consistent with a Middle Miocene to Pliocene initiation of collision between the Greater and Lesser Caucasus. Oligocene to Miocene strata record deposition in a marine environment between the Greater and Lesser Caucasus, while the Greater Caucasus was already undergoing deformation (Vincent et al., 2007), potentially as an accretionary prism. Upper plate (Greater Caucasus) detritus was deposited onto the lower plate (Lesser Caucasus) margin at 15–5.3 Ma, implying subduction/underthrusting of the lower plate basin margin at this time, approximately coeval with a Late Miocene transition to terrestrial sedimentation. Accelerated upper plate exhumation and migration of significant shortening to fold and thrust belt systems occurred around 5.3 Ma, coeval with a transition to erosive conditions in the foreland basin at the locus of collision and deposition of a thick package of upper- and lower plate-derived detritus transported longitudinally. These structural changes and the initiation of erosive foreland conditions suggest a transition in the mode of convergence accommodation from subduction to crustal shortening by 5.3 Ma.

Our results suggest that the lower plate basin margin was subducted at most ~9 Myr prior to the initiation of major crustal shortening associated with the Greater Caucasus–Lesser Caucasus collision, during which <130 km of Lesser Caucasus continental lithosphere could have been subducted. This amount of continental subduction is less than has been proposed for the India–Asia and Arabia–Eurasia collision systems (Ballato et al., 2011; Johnson, 2002; Pirouz et al., 2017). However, the amount inferred for the Caucasus is qualitatively consistent with geodynamic models of collision systems with moderate convergence rates (~7–13 mm/yr) and hot, weak lower plate lithosphere, as inferred in the Caucasus.

Our detrital zircon U-Pb age data also reveal crystallization histories of regional basement terranes, constraining the locations of tectonic sutures. The East European Craton is characterized by zircon ages >900 Ma, while Scythia and the Greater Caucasus basement share subequal

zircon age peaks centred on 450 Ma and 300 Ma, and the Transcaucasus basement is dominated by a 300 Ma age peak and lacks 450 Ma zircon ages. These age distributions suggest sutures between Scythia and the East European Craton and between the Greater Caucasus basement and the Transcaucasus. Scythia, the Greater Caucasus basement, and the Transcaucasus basement all contain zircon grains of 900–600 Ma, characteristic of the Pan-African orogeny on Gondwana. Thus, all three domains likely originated on Gondwana.

ACKNOWLEDGEMENTS

We thank Eric Cowgill, Chad Trexler, Adam Forte, Luka Tsiskarishvili, Salome Gogoladze, Mamuka Natsvlishvili and Rafiq Safarov for field assistance. Tea Godoladze, Fakhraddin Kadirov and Samir Mammadov arranged field logistics. Assistance with sample preparation was provided by Megan Hendrick, Amanda Maslyn, Will Bender and Gordon Moore. Zircon U-Pb analysis was conducted at the University of Arizona Laserchron Center, which is supported by NSF EAR-1338583. We thank Heather Kirkpatrick, Lindsey Abdale, and Laserchron Center staff members Mark Pecha, Dominique Geisler, Kojo Plange, Gayland Simpson, Chelsi White and Dan Alberts for help with zircon U-Pb age analyses. The manuscript was greatly improved by reviews from Matt Malkowski, Douwe van Hinsbergen, Glenn Sharman, Mark Allen and an anonymous reviewer. Nadine McQuarrie is thanked for editorial handling. This work was supported by the University of Michigan via International Institute and Rackham Graduate School grants (ART) and NSF grant EAR-1524304 (NAN). The data that support the findings of this study are available in Supplementary Information Tables S1 and S2 and are also available in the University of Michigan Deep Blue Data repository at <https://doi.org/10.7302/xay7-8a71>. None of the authors have any conflicts of interest to declare.

PEER REVIEW


The peer review history for this article is available at <https://publons.com/publon/10.1111/bre.12499>.

DATA AVAILABILITY STATEMENT

The data that support the findings of this study are available in Supplementary Information Tables S1 and S2 and are also available in the University of Michigan Deep Blue Data repository at <https://doi.org/10.7302/xay7-8a71>.

ORCID

Alexander R. Tye  <https://orcid.org/0000-0002-5573-9115>

Nathan A. Niemi  <https://orcid.org/0000-0002-3380-3024>

REFERENCES

- Abdel-Rahman, A. F. M., & Doig, R. (1987). The Rb-Sr geochronological evolution of the Ras Gharib segment of the northern Nubian Shield. *Journal of the Geological Society*, *144*, 577–586.
- Abdullayev, N. R., Weber, J., van Baak, C. G., Aliyeva, E., Leslie, C., Riley, G. W., ... Kislitsyn, R. (2018). Detrital zircon and apatite constraints on depositional ages, sedimentation rates and provenance: Pliocene Productive Series, South Caspian Basin, Azerbaijan. *Basin Research*, *30*, 835–862.
- Adamia, S., Alania, V., Chabukiani, A., Kutelia, Z., & Sadradze, N. (2011). Great Caucasus (Cavcasioni): A long-lived north-Tethyan back-arc basin. *Turkish Journal of Earth Sciences*, *20*, 611–628.
- Adamia, S., Zakariadze, G., Chkhotua, T., Sadradze, N., Tsereteli, N., Chabukiani, A., & Gventsadze, A. (2011). Geology of the Caucasus: A review. *Turkish Journal of Earth Sciences*, *20*, 489–544.
- Adamia, S. A., Chkhotua, T., Kekelia, M., Lordkipanidze, M., Shavishvili, I., & Zakariadze, G. (1981). Tectonics of the Caucasus and adjoining regions: Implications for the evolution of the Tethys ocean. *Journal of Structural Geology*, *3*, 437–447.
- Aghamalyan, V. (1998). *The crystalline basement of Armenia* (PhD thesis). Institute of Geological Sciences, National Academy of Sciences of Armenia, Yerevan (in Russian).
- Alizadeh, A. A., Guliyev, I. S., Kadirov, F. A., & Eppelbaum, L. V. (2016). *Geosciences of Azerbaijan* (Vol. 1). Heidelberg: Springer.
- Allen, M., Jackson, J., & Walker, R. (2004). Late Cenozoic reorganization of the Arabia-Eurasia collision and the comparison of short-term and long-term deformation rates. *Tectonics*, *23*, TC2008.
- Allen, M. B., & Armstrong, H. A. (2008). Arabia-Eurasia collision and the forcing of mid-Cenozoic global cooling. *Palaeogeography, Palaeoclimatology, Palaeoecology*, *265*, 52–58.
- Allen, M. B., Morton, A. C., Fanning, C. M., Ismail-Zadeh, A. J., & Kroonenberg, S. B. (2006). Zircon age constraints on sediment provenance in the Caspian region. *Journal of the Geological Society*, *163*, 647–655.
- Asch, K. (2005). *IGME 5000: 1 : 5 Million International Geological Map of Europe and Adjacent Areas*. Hannover: BGR.
- Austermann, J., & Iaffaldano, G. (2013). The role of the Zagros orogeny in slowing down Arabia-Eurasia convergence since 5 Ma. *Tectonics*, *32*, 351–363.
- Avdeev, B., & Niemi, N. A. (2011). Rapid Pliocene exhumation of the Central Greater Caucasus constrained by low-temperature thermochronometry. *Tectonics*, *30*, TC2009.
- Avigad, D., Kolodner, K., McWilliams, M., Persing, H., & Weissbrod, T. (2003). Origin of northern Gondwana Cambrian sandstone revealed by detrital zircon SHRIMP dating. *Geology*, *31*, 227–230.
- Axen, G. J., Lam, P. S., Grove, M., Stockli, D. F., & Hassanzadeh, J. (2001). Exhumation of the west-central Alborz Mountains, Iran, Caspian subsidence, and collision-related tectonics. *Geology*, *29*, 559–562.
- Ballato, P., Uba, C. E., Landgraf, A., Strecker, M. R., Sudo, M., Stockli, D. F., ... Tabatabaei, S. H. (2011). Arabia-Eurasia continental collision: Insights from late Tertiary foreland-basin evolution in the Alborz Mountains, northern Iran. *Bulletin*, *123*, 106–131.
- Banks, C. J., Robinson, A. G., & Williams, M. P. (1997). Structure and regional tectonics of the Achara-Trialet fold belt and the adjacent Rioni and Kartli foreland basins, Republic of Georgia. In A. G. Robinson (Ed.), *AAPG Memoir 68: Regional and petroleum geology of the Black Sea and surrounding region* (pp. 331–346).
- Beaumont, C., Ellis, S., Hamilton, J., & Fullsack, P. (1996). Mechanical model for subduction-collision tectonics of Alpine-type compressional orogens. *Geology*, *24*, 675–678.
- Belov, A. (1981). Tectonic evolution of the Alpine folded domain in Paleozoic. *Proceeding of Geological Institute of Academy of Sciences of the USSR*, *347*, 1–212 (in Russian).
- Belov, A., Somin, M., & Adamiya, S. A. (1978). Precambrian and Paleozoic of the Caucasus (brief synthesis). *Jahrbuch fur Geologie und Mineralogie*, *121*, 155–175.
- Bochud, M. (2011). *Tectonics of the Eastern Greater Caucasus in Azerbaijan*. Departement de geosciences, sciences de la terre, Universite de Fribourg.
- Bogdanova, S., Bingen, B., Gorbatshev, R., Kheraskova, T., Kozlov, V., Puchkov, V., & Volozh, Y. A. (2008). The East European Craton (Baltica) before and during the assembly of Rodinia. *Precambrian Research*, *160*, 23–45.
- Burbank, D. W. (1992). Causes of recent Himalayan uplift deduced from deposited patterns in the Ganges basin. *Nature*, *357*, 680–683.
- Carter, D. J., Audley-Charles, M. G., & Barber, A. (1976). Stratigraphical analysis of island arc-continental margin collision in eastern Indonesia. *Journal of the Geological Society*, *132*, 179–198.
- Chemenda, A. I., Mattauer, M., & Bokun, A. N. (1996). Continental subduction and a mechanism for exhumation of high-pressure metamorphic rocks: New modelling and field data from Oman. *Earth and Planetary Science Letters*, *143*, 173–182.
- Chung, S. L., Chu, M. F., Zhang, Y., Xie, Y., Lo, C. H., Lee, T. Y., ... Wang, Y., (2005). Tibetan tectonic evolution inferred from spatial and temporal variations in post-collisional magmatism. *Earth-Science Reviews*, *68*, 173–196.
- Copley, A., & Jackson, J. (2006). Active tectonics of the Turkish-Iranian plateau. *Tectonics*, *25*, TC6006.
- Cowgill, E., Forte, A. M., Niemi, N., Avdeev, B., Tye, A., Trexler, C., ... Godoladze, T. (2016). Relict basin closure and crustal shortening budgets during continental collision: An example from Caucasus sediment provenance. *Tectonics*, *35*, 2918–2947.
- Cowgill, E., Niemi, N. A., Forte, A. M., Trexler, C. C. (2018). Reply to comment by Vincent et al. *Tectonics*, *37*, 1017–1028.
- Şengör, A. C. (1976). Collision of irregular continental margins: Implications for foreland deformation of Alpine-type orogens. *Geology*, *4*, 779–782.
- DeCelles, P. G., Gehrels, G. E., Najman, Y., Martin, A., Carter, A., & Garzanti, E. (2004). Detrital geochronology and geochemistry of Cretaceous-Early Miocene strata of Nepal: Implications for timing and diachroneity of initial Himalayan orogenesis. *Earth and Planetary Science Letters*, *227*, 313–330.
- DeCelles, P. G., & Giles, K. A. (1996). Foreland basin systems. *Basin Research*, *8*, 105–123.
- DeCelles, P. G., Kapp, P., Gehrels, G. E., & Ding, L. (2014). Paleocene-Eocene foreland basin evolution in the Himalaya of southern Tibet and Nepal: Implications for the age of initial India-Asia collision. *Tectonics*, *33*, 824–849.
- Dewey, J., Helman, M., Knott, S., Turco, E., & Hutton, D. (1989). Kinematics of the western Mediterranean. *Geological society* (Vol. 45, pp. 265–283). London, UK: Special Publications.
- Dewey, J., & Mange, M. (1999). Petrography of Ordovician and Silurian sediments in the western Irish Caledonides: Tracers of a short-lived Ordovician continent-arc collision orogeny and the evolution of the

- Laurentian Appalachian-Caledonian margin. *Geological society* (Vol. 164, pp. 55–107). London, UK: Special Publications.
- Dilek, Y., Imamverdiyev, N., & Altunkaynak, Ş. (2010). Geochemistry and tectonics of Cenozoic volcanism in the Lesser Caucasus (Azerbaijan) and the peri-Arabian region: Collision-induced mantle dynamics and its magmatic fingerprint. *International Geology Review*, 52, 536–578.
- Ding, L., Kapp, P., & Wan, X. (2005). Paleocene-Eocene record of ophiolite obduction and initial India-Asia collision, south central Tibet. *Tectonics*, 24, TC3001.
- Dotduduev, S. (1986). On the nappe structure of the Greater Caucasus. *Geotektonika*, 20, 94–106.
- Duffy, B., Quigley, M., Harris, R., & Ring, U. (2013). Arc-parallel extension of the Timor sector of the Banda arc-continent collision. *Tectonics*, 32, 641–660.
- Duretz, T., Gerya, T. V., & May, D. A. (2011). Numerical modelling of spontaneous slab breakoff and subsequent topographic response. *Tectonophysics*, 502, 244–256.
- Duretz, T., Schmalholz, S., & Gerya, T. (2012). Dynamics of slab detachment. *Geochemistry, Geophysics, Geosystems*, 13, Q03020.
- Dzhanelidze, A., & Kandelaki, N. (1957). Geological map of the USSR, Caucasus series sheet K-38-XIII, scale 1:200,000. *Ministry of Geology and Mineral Protection 1369 USSR*, Moscow.
- Edilashvili, V. (1957). Geological map of the USSR, Caucasus series sheet K-38-XXII, scale 1:200,000. *Ministry of Geology and Mineral Protection USSR*, Moscow.
- Edmond, J. (1992). Himalayan tectonics, weathering processes, and the strontium isotope record in marine limestones. *Science*, 258, 1594–1597.
- England, P., & Houseman, G. (1986). Finite strain calculations of continental deformation: 2. Comparison with the India-Asia collision zone. *Journal of Geophysical Research: Solid Earth*, 91, 3664–3676.
- Ershov, A. V., Brunet, M. F., Nikishin, A. M., Bolotov, S. N., Nazarevich, B. P., & Korotaev, M. V. (2003). Northern Caucasus basin: Thermal history and synthesis of subsidence models. *Sedimentary Geology*, 156, 95–118.
- Faccenda, M., Minelli, G., & Gerya, T. (2009). Coupled and decoupled regimes of continental collision: Numerical modeling. *Earth and Planetary Science Letters*, 278, 337–349.
- Fakhari, M. D., Axen, G. J., Horton, B. K., Hassanzadeh, J., & Amini, A. (2008). Revised age of proximal deposits in the Zagros foreland basin and implications for Cenozoic evolution of the High Zagros. *Tectonophysics*, 451, 170–185.
- Fitzgerald, P. G., Roeske, S. M., Benowitz, J. A., Riccio, S. J., Perry, S. E., & Armstrong, P. A. (2014). Alternating asymmetric topography of the Alaska range along the strike slip Denali fault: Strain partitioning and lithospheric control across a terrane suture zone. *Tectonics*, 33, 1519–1533.
- Förster, H. J., Förster, A., Oberhansli, R., & Stromeyer, D. (2010). Lithospheric composition and thermal structure of the Arabian Shield in Jordan. *Tectonophysics*, 481, 29–37.
- Forte, A., Cowgill, E., Bernardin, T., Kreylos, O., & Hamann, B. (2010). Late Cenozoic deformation of the Kura fold-thrust belt, southern Greater Caucasus. *Geological Society of America Bulletin*, 122, 465–486.
- Forte, A. M., & Cowgill, E. (2013). Late Cenozoic base-level variations of the Caspian Sea: A review of its history and proposed driving mechanisms. *Palaeogeography, Palaeoclimatology, Palaeoecology*, 386, 392–407.
- Forte, A. M., Cowgill, E., Murtuzayev, I., Kangarli, T., & Stoica, M. (2013). Structural geometries and magnitude of shortening in the eastern Kura fold-thrust belt, Azerbaijan: Implications for the development of the Greater Caucasus Mountains. *Tectonics*, 32, 688–717.
- Forte, A. M., Cowgill, E., & Whipple, K. X. (2014). Transition from a singly vergent to doubly vergent wedge in a young orogen: The Greater Caucasus. *Tectonics*, 33, 2077–2101.
- Galoyan, G., Rolland, Y., Sosson, M., Corsini, M., Billo, S., Verati, C., & Melkonyan, R. (2009). Geology, geochemistry and ⁴⁰Ar/³⁹Ar dating of Sevan ophiolites (Lesser Caucasus, Armenia): Evidence for Jurassic back-arc opening and hot spot event between the South Armenian Block and Eurasia. *Journal of Asian Earth Sciences*, 34, 135–153.
- Gamkrelidze, I. P., & Shengelia, D. M. (2007). Pre-Alpine geodynamics of the Caucasus, suprasubduction regional metamorphism and granitoid magmatism. *Bulletin of the Georgian National Academy of Sciences*, 175, 57–65.
- Gamkrelidze, P., & Kakhadze, I. (1959). Geological map of the USSR, Caucasus series sheet K-38-VII, scale 1:200,000. *Ministry of Geology and Mineral Protection USSR*, Moscow.
- Garzanti, E., Baud, A., & Mascle, G. (1987). Sedimentary record of the northward flight of India and its collision with Eurasia (Ladakh Himalaya, India). *Geodinamica Acta*, 1, 297–312.
- Gehrels, G. E., Valencia, V. A., & Ruiz, J. (2008). Enhanced precision, accuracy, efficiency, and spatial resolution of U-Pb ages by laser ablation–multicollector–inductively coupled plasma–mass spectrometry. *Geochemistry, Geophysics, Geosystems*, 9(3).
- Göğüş, O. H., & Pysklywec, R. N. (2008). Mantle lithosphere delamination driving plateau uplift and synconvergent extension in eastern Anatolia. *Geology*, 36, 723–726.
- Green, T., Abdullayev, N., Hossack, J., Riley, G., & Roberts, A. M. (2009). Sedimentation and subsidence in the south Caspian Basin, Azerbaijan. *Geological society* (Vol. 312, pp. 241–260). London, UK: Special Publications.
- Gürer, D., & van Hinsbergen, D. J. (2019). Diachronous demise of the Neotethys Ocean as a driver for non-cylindrical orogenesis in Anatolia. *Tectonophysics*, 760, 95–106.
- Hess, J., Aretz, J., Gurbanov, A., Emmermann, R., & Lippolt, H. (1995). Subduction related Jurassic andesites in the northern Great Caucasus. *Geologische Rundschau*, 84, 319–333.
- Hinds, D., Aliyeva, E., Allen, M., Davies, C., Kroonenberg, S., Simmons, M., & Vincent, S. (2004). Sedimentation in a discharge dominated fluvial-lacustrine system: The Neogene Productive Series of the South Caspian Basin, Azerbaijan. *Marine and Petroleum Geology*, 21, 613–638.
- Höhndorf, A., Meinhold, K., & Vail, J. (1994). Geochronology of anorogenic igneous complexes in the Sudan: Isotopic investigations in North Kordofan, the Nubian Desert and the Red Sea Hills. *Journal of African Earth Sciences*, 19, 3–15.
- Horton, B., Hassanzadeh, J., Stockli, D., Axen, G., Gillis, R., Guest, B., ... Grove, M. (2008). Detrital zircon provenance of Neoproterozoic to Cenozoic deposits in Iran: Implications for chronostratigraphy and collisional tectonics. *Tectonophysics*, 451, 97–122.
- Hu, X., Garzanti, E., Moore, T., & Raffi, I. (2015). Direct stratigraphic dating of India-Asia collision onset at the Selandian (middle Paleocene, 59 ± 1 ma). *Geology*, 43, 859–862.
- Hu, X., Sinclair, H. D., Wang, J., Jiang, H., & Wu, F. (2012). Late Cretaceous-Palaeogene stratigraphic and basin evolution in the Zhepure Mountain of southern Tibet: Implications for the timing of India-Asia initial collision. *Basin Research*, 24, 520–543.

- Hudson, S. M., Johnson, C. L., Efendiyeva, M. A., Rowe, H. D., Feyzullayev, A. A., & Aliyev, C. S. (2008). Stratigraphy and geochemical characterization of the Oligocene-Miocene Maikop series: Implications for the paleogeography of Eastern Azerbaijan. *Tectonophysics*, *451*, 40–55.
- Hurford, A., Fitch, F., & Clarke, A. (1984). Resolution of the age structure of the detrital zircon populations of two Lower Cretaceous sandstones from the Weald of England by fission track dating. *Geological Magazine*, *121*, 269–277.
- Jagoutz, O., Macdonald, F. A., & Royden, L. (2016). Low-latitude arc-continent collision as a driver for global cooling. *Proceedings of the National Academy of Sciences*, *113*, 4935–4940.
- Johnson, M. (2002). Shortening budgets and the role of continental subduction during the India-Asia collision. *Earth-Science Reviews*, *59*, 101–123.
- Johnson, P. R. (2014). An expanding Arabian-Nubian Shield geochronologic and isotopic dataset: Defining limits and confirming the tectonic setting of a Neoproterozoic accretionary orogen. *The Open Geology Journal*, *8*, 3–33.
- Johnson, P. R., & Woldehaimanot, B. (2003). Development of the Arabian-Nubian Shield: Perspectives on accretion and deformation in the northern East African Orogen and the assembly of Gondwana. *Geological Society* (Vol. 206, pp. 289–325). London, UK: Special Publications.
- Jones, R., & Simmons, M. (1997). A review of the stratigraphy of eastern Paratethys (Oligocene-Holocene), with particular emphasis on the Black Sea, in Regional and Petroleum Geology of the Black Sea and Surrounding Regions. In A. Robinson (Ed.), *American Association of Petroleum Geologists Memoir* (Vol. 68, pp. 39–52).
- Jones, R. R., & Tanner, P. G. (1995). Strain partitioning in transpression zones. *Journal of Structural Geology*, *17*, 793–802.
- Kadirov, F., Floyd, M., Alizadeh, A., Guliev, I., Reilinger, R., Kuleli, S., ... Toksoz, M. N. (2012). Kinematics of the eastern Caucasus near Baku, Azerbaijan. *Natural Hazards*, *63*, 997–1006.
- Kadirov, F., Floyd, M., Reilinger, R., Alizadeh, A. A., Guliyev, I., Mammadov, S., & Safarov, R. (2015). Active geodynamics of the Caucasus region: Implications for earthquake hazards in Azerbaijan. *Proceedings of Azerbaijan National Academy of Sciences, The Sciences of Earth*, *3*, 3–17.
- Kangarli, T., Kadirov, F., Yetirmishli, G., Aliyev, F., Kazimova, S., Aliyev, M., Safarov, R., ... Vahabov, U. (2018). Recent geodynamics, active faults and earthquake focal mechanisms of the zone of pseudosubduction interaction between the Northern and Southern caucasus microplates in the southern slope of the Greater Caucasus (Azerbaijan). *Geodynamics & Tectonophysics*, *9*, 1099–1126.
- Karig, D. E., & Sharman, G. F. (1975). Subduction and accretion in trenches. *Geological Society of America Bulletin*, *86*, 377–389.
- Keskin, M., Pearce, J. A., & Mitchell, J. (1998). Volcano-stratigraphy and geochemistry of collision-related volcanism on the Erzurum-Kars Plateau, northeastern Turkey. *Journal of Volcanology and Geothermal Research*, *85*, 355–404.
- Khain, V. (1975). Structure and main stages in the tectono-magmatic development of the Caucasus: An attempt at geodynamic interpretation. *American Journal of Science*, *275*, 131–156.
- Khain, V., Gadjev, A., & Kengerli, T. (2007). Tectonic origin of the Apsheron threshold in the Caspian Sea. In *Doklady earth sciences* (p. 552). Dordrecht: Springer Nature BV.
- Khain, V., & Shardanov, A. (1960). Geological map of the USSR, Caucasus series sheet K-39-XXV, scale 1:200,000. *Ministry of Geology and Mineral Protection USSR*, Moscow.
- Klootwijk, C., Conaghan, P., & Powell, C. M. (1985). The Himalayan Arc: Large-scale continental subduction, oroclinal bending and back-arc spreading. *Earth and Planetary Science Letters*, *75*, 167–183.
- Knapp, C. C., Knapp, J. H., & Connor, J. A. (2004). Crustal-scale structure of the South Caspian Basin revealed by deep seismic reflection profiling. *Marine and Petroleum Geology*, *21*, 1073–1081.
- Knipper, A., & Khain, E. (1980). Structural position of ophiolites of the Caucasus. *Ofioliti*, *2*, 297–314.
- Kopp, M. (1985). Age and nature of deformations of sediments comprising the Lagich syncline (southeastern Caucasus). *Geologiya*, *40*, 25–34.
- Kopp, M., & Shcherba, I. (1985). Late Alpine development of the east Caucasus. *Geotectonics*, *19*, 497–507.
- Koshnaw, R. I., Stockli, D. F., & Schlunegger, F. (2019). Timing of the Arabia-Eurasia continental collision: Evidence from detrital zircon U-Pb geochronology of the Red Bed Series strata of the northwest Zagros hinterland, Kurdistan region of Iraq. *Geology*, *47*, 47–50.
- Krijgsman, W., Hilgen, F., Raffi, I., Sierro, F. J., & Wilson, D. (1999). Chronology, causes and progression of the Messinian salinity crisis. *Nature*, *400*, 652.
- Krijgsman, W., Stoica, M., Vasiliev, I., & Popov, V. (2010). Rise and fall of the Paratethys Sea during the Messinian Salinity Crisis. *Earth and Planetary Science Letters*, *290*, 183–191.
- Lallemant, S. E., Malavieille, J., & Calassou, S. (1992). Effects of oceanic ridge subduction on accretionary wedges: Experimental modeling and marine observations. *Tectonics*, *11*, 1301–1313.
- Lee, T. Y., & Lawver, L. A. (1995). Cenozoic plate reconstruction of Southeast Asia. *Tectonophysics*, *251*, 85–138.
- Lipman, P. W., Bogatkov, O., Tsvetkov, A., Gazis, C., Gurbanov, A. G., Hon, K., ... Marchev, P. (1993). 2.8-Ma ash-flow caldera at Chegem River in the northern Caucasus Mountains (Russia), contemporaneous granites, and associated ore deposits. *Journal of Volcanology and Geothermal Research*, *57*, 85–124.
- Madanipour, S., Ehlers, T. A., Yassaghi, A., & Enkelmann, E. (2017). Accelerated middle Miocene exhumation of the Talesh Mountains constrained by U-Th/He thermochronometry: Evidence for the Arabia-Eurasia collision in the NW Iranian Plateau. *Tectonics*, *36*, 1538–1561.
- Malkowski, M. A., Schwartz, T. M., Sharman, G. R., Sickmann, Z. T., & Graham, S. A. (2017). Stratigraphic and provenance variations in the early evolution of the Magallanes-Austral foreland basin: Implications for the role of longitudinal versus transverse sediment dispersal during arc-continent collision. *Bulletin*, *129*, 349–371.
- Mangino, S., & Priestley, K. (1998). The crustal structure of the southern Caspian region. *Geophysical Journal International*, *133*, 630–648.
- Mayringer, F., Treloar, P. J., Gerdes, A., Finger, F., & Shengelia, D. (2011). New age data from the Dzirula massif, Georgia: Implications for the evolution of the Caucasian Variscides. *American Journal of Science*, *311*, 404–441.
- McQuarrie, N., Stock, J., Verdel, C., & Wernicke, B. (2003). Cenozoic evolution of Neotethys and implications for the causes of plate motions. *Geophysical Research Letters*, *30*, 2036.
- Mekhtiev, S., Gorin, V., Agabekov, M., & Voronin, M. (1962). Geological map of the USSR, Caucasus series sheet K-39-XXXII, scale 1:200,000. *Ministry of Geology and Mineral Protection USSR*, Moscow.

- Mellors, R., Jackson, J., Myers, S., Gok, R., Priestley, K., Yetirmishli, G., & Godoladze, T. (2012). Deep earthquakes beneath the Northern Caucasus: Evidence of active or recent subduction in western Asia. *Bulletin of the Seismological Society of America*, *102*, 862–866.
- Mengel, K., Borsuk, A., Gurbanov, A., Wedepohl, K., Baumann, A., & Hoefs, J. (1987). Origin of spilitic rocks from the southern slope of the Greater Caucasus. *Lithos*, *20*, 115–133.
- Molnar, P., Boos, W. R., & Battisti, D. S. (2010). Orographic controls on climate and paleoclimate of Asia: Thermal and mechanical roles for the Tibetan Plateau. *Annual Review of Earth and Planetary Sciences*, *38*, 77–102.
- Morton, A., Allen, M., Simmons, M., Spathopoulos, F., Still, J., Hinds, D., & Kroonenberg, S. (2003). Provenance patterns in a neotectonic basin: Pliocene and Quaternary sediment supply to the South Caspian. *Basin Research*, *15*, 321–337.
- Mumladze, T., Forte, A. M., Cowgill, E. S., Trexler, C. C., Niemi, N. A., Yikilmaz, M. B., & Kellogg, L. H. (2015). Subducted, detached, and torn slabs beneath the Greater Caucasus. *GeoResJ*, *5*, 36–46.
- Najman, Y., Appel, E., Boudagher-Fadel, M., Bown, P., Carter, A., Garzanti, E., Parrish, R. (2010). Timing of India-Asia collision: Geological, biostratigraphic, and palaeomagnetic constraints. *Journal of Geophysical Research: Solid Earth*, *115*, B12416.
- Nalivkin, D. (1976). Geologic Map of the Caucasus (in Russian). scale 1: 500,000. *Ministry of Geology, USSR*, Moscow.
- Nance, R. D., Murphy, J. B., & Santosh, M. (2014). The supercontinent cycle: A retrospective essay. *Gondwana Research*, *25*, 4–29.
- Natal'in, B. A., & Şengör, A. C. (2005). Late Palaeozoic to Triassic evolution of the Turan and Scythian platforms: The pre-history of the Palaeo-Tethyan closure. *Tectonophysics*, *404*, 175–202.
- Nazarevich, B., Nazarevich, I., & Shvydko, N. (1986). The Upper Triassic Nogai volcano sedimentary formation of Eastern Fore-Caucasus: Composition, constitution, and relations to earlier and later-formed volcanics. *The Formations of Sedimentary Basins*. Nauka, Moscow (In Russian), 67–86.
- Nikishin, A. M., Okay, A. I., Tuysuz, O., Demirer, A., Amelin, N., & Petrov, E. (2015). The Black Sea basins structure and history: New model based on new deep penetration regional seismic data. Part 1: Basins structure and fill. *Marine and Petroleum Geology*, *59*, 638–655.
- Patriat, P., & Achache, J. (1984). India-Eurasia collision chronology has implications for crustal shortening and driving mechanism of plates. *Nature*, *311*, 615.
- Perchuk, A., & Philippot, P. (1997). Rapid cooling and exhumation of eclogitic rocks from the Great Caucasus, Russia. *Journal of Metamorphic Geology*, *15*, 299–310.
- Phillip, H., Cisternas, A., Gvishiani, A., & Gorshkov, A. (1989). The Caucasus: An actual example of the initial stages of continental collision. *Tectonophysics*, *161*, 1–21.
- Philippot, P., Blichert-Toft, J., Perchuk, A., Costa, S., & Gerasimov, V. (2001). Lu-Hf and Ar-Ar chronometry supports extreme rate of subduction zone metamorphism deduced from geospeedometry. *Tectonophysics*, *342*, 23–38.
- Pirouz, M., Avouac, J. P., Hassanzadeh, J., Kirschvink, J. L., & Bahrudi, A. (2017). Early Neogene foreland of the Zagros, implications for the initial closure of the Neo-Tethys and kinematics of crustal shortening. *Earth and Planetary Science Letters*, *477*, 168–182.
- Popov, S. V., Shcherba, I. G., Ilyina, L. B., Nevesskaya, L. A., Paramonova, N. P., Khondkarian, S. O., & Magyar, I. (2006). Late Miocene to Pliocene palaeogeography of the Paratethys and its relation to the Mediterranean. *Palaeogeography, Palaeoclimatology, Palaeoecology*, *238*, 91–106.
- Pullen, A., Ibáñez-Mejía, M., Gehrels, G. E., Ibáñez-Mejía, J. C., & Pecha, M. (2014). What happens when n= 1000? Creating large-n geochronological datasets with LA-ICP-MS for geologic investigations. *Journal of Analytical Atomic Spectrometry*, *29*(6), 971–980.
- Pusok, A., & Kaus, B. J. (2015). Development of topography in 3-D continental-collision models. *Geochemistry, Geophysics, Geosystems*, *16*, 1378–1400.
- Raines, M. K., Hubbard, S. M., Kukulski, R. B., Leier, A. L., & Gehrels, G. E. (2013). Sediment dispersal in an evolving foreland: Detrital zircon geochronology from Upper Jurassic and lowermost Cretaceous strata, Alberta Basin, Canada. *Geological Society of America Bulletin*, *125*, 741–755.
- Regard, V., Faccenna, C., Martinod, J., Bellier, O., & Thomas, J. C. (2003). From subduction to collision: Control of deep processes on the evolution of convergent plate boundary. *Journal of Geophysical Research: Solid Earth*, *108*, 2208.
- Reilinger, R., McClusky, S., Vernant, P., Lawrence, S., Ergintav, S., Cakmak, R., ... Nadariya, M. (2006). GPS constraints on continental deformation in the Africa-Arabia-Eurasia continental collision zone and implications for the dynamics of plate interactions. *Journal of Geophysical Research: Solid Earth*, *111*, B05411.
- Rolland, Y., Hassig, M., Bosch, D., Meijers, M., Sosson, M., Bruguier, O., ... Sadradze, N. (2016). A review of the plate convergence history of the East Anatolia-Transcaucasus region during the Variscan: Insights from the Georgian basement and its connection to the Eastern Pontides. *Journal of Geodynamics*, *96*, 131–145.
- Rolland, Y., Perincek, D., Kaymakci, N., Sosson, M., Barrier, E., & Avagyan, A. (2012). Evidence for 80.75 Ma subduction jump during Anatolide-Tauride-Armenian block accretion and 48 Ma Arabia-Eurasia collision in Lesser Caucasus-East Anatolia. *Journal of Geodynamics*, *56*, 76–85.
- Rolland, Y., Sosson, M., Adamia, S., & Sadradze, N. (2011). Prolonged Variscan to Alpine history of an active Eurasian margin (Georgia, Armenia) revealed by 40Ar/39Ar dating. *Gondwana Research*, *20*, 798–815.
- Ruban, D. (2007). Major Paleozoic-Mesozoic unconformities in the Greater Caucasus and their tectonic re-interpretation: A synthesis. *GeoActa*, *6*, 91–102.
- Ruban, D. (2013). The Greater Caucasus-A Galatian or Hanseatic terrane: Comment on 'the formation of pangea' by GM Stampfli, C. Hochard, C. Verard, C. Wilhem and J. von Raumer. *Tectonophysics*, *593*, 1–19.
- Ruban, D. A., Zerkov, H., & Yang, W. (2007). A new hypothesis on the position of the Greater Caucasus Terrane in the Late Palaeozoic-Early Mesozoic based on palaeontologic and lithologic data. *Trabajos de Geologia*, *27*, 19–27.
- Rusmore, M. E., Gehrels, G., & Woodsworth, G. (2001). Southern continuation of the Coast shear zone and Paleocene strain partitioning in British Columbia-southeast Alaska. *Geological Society of America Bulletin*, *113*, 961–975.
- Sahakyan, L., Bosch, D., Sosson, M., Avagyan, A., Galoyan, G., Rolland, Y., ... Vardanyan, S. (2017). Geochemistry of the Eocene magmatic rocks from the Lesser Caucasus area (Armenia): Evidence of a subduction geodynamic environment. *Geological society* (Vol. 428, pp. 73–98). London, UK: Special Publications.
- Saintot, A., Brunet, M. F., Yakovlev, F., Sebrier, M., Stephenson, R., Ershov, A., & McCann, T. (2006). The Mesozoic-Cenozoic tectonic

- evolution of the Greater Caucasus. *Geological society* (Vol. 32, 277–289). London, Memoirs.
- Saintot, A., Stephenson, R. A., Stovba, S., Brunet, M. F., Yegorova, T., & Starostenko, V. (2006). The evolution of the southern margin of Eastern Europe (Eastern European and Scythian platforms) from the latest Precambrian-Early Palaeozoic to the Early Cretaceous. *Geological society* (Vol. 32, pp. 481–505). London, Memoirs.
- Şengör, A., & Kidd, W. (1979). Post-collisional tectonics of the Turkish-Iranian plateau and a comparison with Tibet. *Tectonophysics*, 55, 361–376.
- Şengör, A., Ozeren, S., Genc, T., & Zor, E. (2003). East Anatolian high plateau as a mantle-supported, north-south shortened domal structure. *Geophysical Research Letters*, 30, 8045.
- Şengör, A., & Yılmaz, Y. (1981). Tethyan evolution of Turkey: A plate tectonic approach. *Tectonophysics*, 75, 181–241.
- Şengör, A., Yılmaz, Y., & Sungurlu, O. (1984). Tectonics of the Mediterranean Cimmerides: Nature and evolution of the western termination of Palaeo-Tethys. *Geological society* (Vol. 17, pp. 77–112). London, UK: Special Publications.
- Şengör, A. C. (1984). The Cimmeride orogenic system and the tectonics of Eurasia. *Geological Society of America Special Papers*, 195, 1–74.
- Sengupta, S., Corfu, F., McNutt, R., & Paul, D. (1996). Mesoarchean crustal history of the eastern Indian craton: Sm-Nd and U-Pb isotopic evidence. *Precambrian Research*, 77, 17–22.
- Shimazaki, H., & Shinomoto, S. (2010). Kernel bandwidth optimization in spike rate estimation. *Journal of Computational Neuroscience*, 29, 171–182.
- Sholpo, V. (1978). *Alpine Geodynamics of the Greater Caucasus (in Russian)* (p. 176). Moscow, Russia: Nedra
- Silverman, B. W. (1986). *Density estimation for statistics and data analysis* (Vol. 26). New York, London: CRC Press.
- Skobel'tsyn, G., Mellors, R., Gok, R., Turkelli, N., Yetirmishli, G., & Sandvol, E. (2014). Upper mantle S wave velocity structure of the East Anatolian-Caucasus region. *Tectonics*, 33, 207–221.
- Sobornov, K. O. (1994). Structure and petroleum potential of the Dagestan thrust belt, northeastern Caucasus, Russia. *Bulletin of Canadian Petroleum Geology*, 42, 352–364.
- Sobornov, K. O. (1996). Lateral variations in structural styles of tectonic wedging in the northeastern Caucasus, Russia. *Bulletin of Canadian Petroleum Geology*, 44, 385–399.
- Sokhadze, G., Floyd, M., Godoladze, T., King, R., Cowgill, E., Javakishvili, Z., ... Reilinger, R. (2018). Active convergence between the Lesser and Greater Caucasus in Georgia: Constraints on the tectonic evolution of the Lesser-Greater Caucasus continental collision. *Earth and Planetary Science Letters*, 481, 154–161.
- Somin, M. L. (2011). Pre-Jurassic basement of the Greater Caucasus: Brief overview. *Turkish Journal of Earth Sciences*, 20, 545–610.
- Soria, J., Fernandez, J., & Viseras, C. (1999). Late Miocene stratigraphy and palaeogeographic evolution of the intramontane Guadix Basin (Central Betic Cordillera, Spain): Implications for an Atlantic-Mediterranean connection. *Palaeogeography, Palaeoclimatology, Palaeoecology*, 151, 255–266.
- Sosson, M., Rolland, Y., Muller, C., Danelian, T., Melkonyan, R., Kekelia, S., ... Galoyan, G. (2010). Subductions, obduction and collision in the Lesser Caucasus (Armenia, Azerbaijan, Georgia), new insights. *Geological society* (Vol. 340, pp. 329–352). London, UK: Special Publications.
- Stampfli, G., Hochard, C., Verard, C., & Wilhem, C. (2013). The formation of Pangea. *Tectonophysics*, 593, 1–19.
- Stampfli, G. M. (2013). Response to the comments on “the formation of Pangea” by DA Ruban. *Tectonophysics*, 608, 1445–1447.
- Stampfli, G. M., & Borel, G. (2002). A plate tectonic model for the Paleozoic and Mesozoic constrained by dynamic plate boundaries and restored synthetic oceanic isochrons. *Earth and Planetary Science Letters*, 196, 17–33.
- Stern, R. J., & Johnson, P. (2010). Continental lithosphere of the Arabian Plate: A geologic, petrologic, and geophysical synthesis. *Earth-Science Reviews*, 101, 29–67.
- Tate, G. W., McQuarrie, N., van Hinsbergen, D. J., Bakker, R. R., Harris, R., & Jiang, H. (2015). Australia going down under: Quantifying continental subduction during arc-continent accretion in Timor-Leste. *Geosphere*, 11, 1860–1883.
- Teng, L. S. (1990). Geotectonic evolution of late Cenozoic arc-continent collision in Taiwan. *Tectonophysics*, 183, 57–76.
- Topuz, G., Candan, O., Zack, T., & Yılmaz, A. (2017). East Anatolian plateau constructed over a continental basement: No evidence for the East Anatolian accretionary complex. *Geology*, 45, 791–794.
- Toussaint, G., Burov, E., & Avouac, J. P. (2004). Tectonic evolution of a continental collision zone: A thermomechanical numerical model. *Tectonics*, 23, TC6003.
- Toussaint, G., Burov, E., & Jolivet, L. (2004). Continental plate collision: Unstable vs. stable slab dynamics. *Geology*, 32, 33–36.
- Trexler, C. C. (2018). *Structural Investigations of the Tectonic History of the Western Greater Caucasus Mountains*. Republic of Georgia: University of California, Davis.
- Tricart, P. (1984). From passive margin to continental collision; a tectonic scenario for the Western Alps. *American Journal of Science*, 284, 97–120.
- Tye, A., Wolf, A., & Niemi, N. (2019). Bayesian population correlation: A probabilistic approach to inferring and comparing population distributions for detrital zircon ages. *Chemical Geology*, 518, 67–78.
- van Baak, C. G., Grothe, A., Richards, K., Stoica, M., Aliyeva, E., Davies, G. R., ... Krijgsman, W. (2019). Flooding of the Caspian Sea at the intensification of Northern Hemisphere Glaciations. *Global and Planetary Change*, 174, 153–163.
- van Baak, C. G., Krijgsman, W., Magyar, I., Sztano, O., Golovina, L. A., Grothe, A., ... Radionova, E. P. (2017). Paratethys response to the Messinian salinity crisis. *Earth-Science Reviews*, 172, 193–223.
- van Baak, C. G., Radionova, E. P., Golovina, L. A., Raffi, I., Kuiper, K. F., Vasiliev, I., & Krijgsman, W. (2015). Messinian events in the Black Sea. *Terra Nova*, 27, 433–441.
- van der Boon, A., van Hinsbergen, D., Rezaeian, M., Gurer, D., Honarmand, M., Pastor-Galan, D., ... Langereis, C. (2018). Quantifying Arabia-Eurasia convergence accommodated in the Greater Caucasus by paleomagnetic reconstruction. *Earth and Planetary Science Letters*, 482, 454–469.
- van Der Boon, A., Kuiper, K., Villa, G., Renema, W., Meijers, M., Langereis, C., ... Krijgsman, W. (2017). Onset of Maikop sedimentation and cessation of Eocene arc volcanism in the Talys Mountains, Azerbaijan. *Geological society* (Vol. 428, pp. 145–169). London, UK: Special Publications.
- van Hinsbergen, D. J., Lippert, P. C., Dupont-Nivet, G., McQuarrie, N., Doubrovine, P. V., Spakman, W., & Torsvik, T. H. (2012). Greater India Basin hypothesis and a two-stage Cenozoic collision between India and Asia. *Proceedings of the National Academy of Sciences*, 109, 7659–7664.
- van Hinsbergen, D. J., Torsvik, T. H., Schmid, S. M., MaiCtenco, L. C., Maffione, M., Vissers, R. L., ... Spakman, W. (2020). Orogenic

- architecture of the Mediterranean region and kinematic reconstruction of its tectonic evolution since the Triassic. *Gondwana Research*, 81, 79–229.
- Vasey, D., Cowgill, E., Roeske, S., Niemi, N., Godoladze, T., Skhirtladze, I., & Gogoladze, S. (2020). Evolution of the Greater Caucasus basement and formation of the Main Caucasus Thrust Georgia. *Tectonics*, e2019TC005828.
- Vasiliev, I., Reichart, G. J., & Krijgsman, W. (2013). Impact of the Messinian Salinity Crisis on Black Sea hydrology: Insights from hydrogen isotopes analysis on biomarkers. *Earth and Planetary Science Letters*, 362, 272–282.
- Verdel, C., Wernicke, B. P., Hassanzadeh, J., & Guest, B. (2011). A Paleogene extensional arc flare-up in Iran. *Tectonics*, 30, TC3008.
- Vermeesch, P. (2012). On the visualisation of detrital age distributions. *Chemical Geology*, 312, 190–194.
- Vincent, S. J., Braham, W., Lavrishchev, V. A., Maynard, J. R., & Harland, M. (2016). The formation and inversion of the western Greater Caucasus Basin and the uplift of the western Greater Caucasus: Implications for the wider Black Sea region. *Tectonics*, 35, 2948–2962.
- Vincent, S. J., Carter, A., Lavrishchev, V. A., Rice, S. P., Barabadze, T. G., & Hovius, N. (2011). The exhumation of the western Greater Caucasus: A thermochronometric study. *Geological Magazine*, 148, 1–21.
- Vincent, S. J., Davies, C. E., Richards, K., & Aliyeva, E. (2010). Contrasting Pliocene fluvial depositional systems within the rapidly subsiding South Caspian Basin; a case study of the palaeo-Volga and palaeo-Kura river systems in the Surakhany Suite, Upper Productive Series, onshore Azerbaijan. *Marine and Petroleum Geology*, 27, 2079–2106.
- Vincent, S. J., Hyden, F., & Braham, W. (2014). Along-strike variations in the composition of sandstones derived from the uplifting western Greater Caucasus: Causes and implications for reservoir quality prediction in the Eastern Black Sea. *Geological society* (Vol. 386, 111–127). London, UK: Special Publications.
- Vincent, S. J., Morton, A. C., Carter, A., Gibbs, S., & Barabadze, T. G. (2007). Oligocene uplift of the Western Greater Caucasus: An effect of initial Arabia-Eurasia collision. *Terra Nova*, 19, 160–166.
- Vincent, S. J., Morton, A. C., Hyden, F., & Fanning, M. (2013). Insights from petrography, mineralogy and U-Pb zircon geochronology into the provenance and reservoir potential of Cenozoic siliciclastic depositional systems supplying the northern margin of the Eastern Black Sea. *Marine and Petroleum Geology*, 45, 331–348.
- Vincent, S. J., Saintot, A., Mosar, J., Okay, A. I., & Nikishin, A. M. (2018). Comment on 'relict basin closure and crustal shortening budgets during continental collision: An example from Caucasus sediment provenance' by Cowgill et al. (2016). *Tectonics* 37, 1006–1016.
- Vincent, S. J., Somin, M. L., Carter, A., Vezzoli, G., Fox, M., & Vautravers, B. (2020). Testing models of Cenozoic exhumation in the western Greater Caucasus. *Tectonics*, 39(2), e2018TC005451.
- Voronin, M., Gavrilov, M., & Khain, V. (1959). Geological map of the USSR, Caucasus series sheet K-39-XXXI, scale 1:200,000. *Ministry of Geology and Mineral Protection USSR*, Moscow.
- Wang, C. Y., Campbell, I. H., Stepanov, A. S., Allen, C. M., & Burtsev, I. N. (2011). Growth rate of the preserved continental crust: II. Constraints from Hf and O isotopes in detrital zircons from Greater Russian Rivers. *Geochimica et Cosmochimica Acta*, 75, 1308–1345.
- Weislogel, A. L., Graham, S. A., Chang, E. Z., Wooden, J. L., Gehrels, G. E., & Yang, H. (2006). Detrital zircon provenance of the Late Triassic Songpan-Ganzi complex: Sedimentary record of collision of the North and South China blocks. *Geology*, 34, 97–100.
- Wu, F. Y., Ji, W. Q., Wang, J. G., Liu, C. Z., Chung, S. L., & Clift, P. D. (2014). Zircon U-Pb and Hf isotopic constraints on the onset time of India-Asia collision. *American Journal of Science*, 314, 548–579.
- Yılmaz, A., Adamia, S., & Yılmaz, H. (2014). Comparisons of the suture zones along a geotraverse from the Scythian Platform to the Arabian Platform. *Geoscience Frontiers*, 5, 855–875.
- Zagorevski, A., & van Staal, C. (2011). The record of Ordovician arc-arc and arc-continent collisions in the Canadian Appalachians during the closure of Iapetus. In *Arc-continent collision* (pp. 341–371). Berlin, Heidelberg: Springer.
- Zakariadze, G. S., Dilek, Y., Adamia, S. A., Oberhansli, R., Karpenko, S., Bazylev, B., & Solovüfeva, N. (2007). Geochemistry and geochronology of the Neoproterozoic Pan-African Transcaucasian Massif (Republic of Georgia) and implications for island arc evolution of the late Precambrian Arabian-Nubian Shield. *Gondwana Research*, 11, 92–108.
- Zhuang, G., Najman, Y., Guillot, S., Roddaz, M., Antoine, P. O., Metais, G., ... Solangi, S. H. (2015). Constraints on the collision and the pre-collision tectonic configuration between India and Asia from detrital geochronology, thermochronology, and geochemistry studies in the lower Indus basin, Pakistan. *Earth and Planetary Science Letters*, 432, 363–373.
- Zonenshain, L. P., & Le Pichon, X. (1986). Deep basins of the Black Sea and Caspian Sea as remnants of Mesozoic back-arc basins. *Tectonophysics*, 123, 181–211.
- Zubakov, V. (2001). History and causes of variations in the Caspian Sea level: The Miopliocene, 7.1.1.95 million years ago. *Water Resources*, 28, 249–256.

SUPPORTING INFORMATION

Additional Supporting Information may be found online in the Supporting Information section.

How to cite this article: Tye AR, Niemi NA, Safarov RT, Kadirov FA, Babayev GR. Sedimentary response to a collision orogeny recorded in detrital zircon provenance of Greater Caucasus foreland basin sediments. *Basin Res.* 2021;33:933–967. <https://doi.org/10.1111/bre.12499>